Chapter 8. *In vitro* and *in silico* analysis of the influence of D_2 antagonist target binding kinetics on the cellular response to fluctuating dopamine concentrations

Wilhelmus E. A. de Witte[1], Joost W. Versfelt[1], Maria Kuzikov[2], Solene Rolland[3], Victoria Georgi[3], Philip Gribbon[2], Sheraz Gul[2], Dymphy Huntjens[4], Piet Hein van der Graaf[1,5], Meindert Danhof[1], Amaury Fernández-Montalván[3], Gesa Witt[2], Elizabeth C. M. de Lange[1*].

[1] Division of Pharmacology, Leiden Academic Centre for Drug Research, Leiden University, 2333 CC Leiden, The Netherlands

[2] Fraunhofer Institute for Molecular Biology and Applied Ecology, ScreeningPort, Hamburg, Germany

[3] Bayer Healthcare Pharmaceuticals, Global Drug Discovery, Berlin, Germany

[4] Janssen R&D, Janssen Pharmaceutica, Beerse, Belgium

[5] Certara Quantitative Systems Pharmacology, Canterbury Innovation Centre, Canterbury CT2 7FG, United Kingdom

* Correspondence: ecmdelange@lacdr.leidenuniv.nl

Manuscript under revision for the British Journal of Pharmacology

Abstract

Introduction

Target binding kinetics can influence the time course of the drug effect (pharmacodynamics) both I) directly, by affecting the time course of target occupancy, driven by the pharmacokinetics of the drug, competition with endogenous ligands and target turnover, and II) indirectly, by affecting signal transduction and homeostatic feedback at the cellular and systems level. For dopamine D_2 antagonists, it has been hypothesized that fast receptor binding kinetics cause fewer side effects, because part of the dynamics of the dopaminergic system is preserved by displacement of these antagonists.

Methods

Target binding kinetics of D_2 antagonists and agonists and signal transduction after dopamine and D_2 antagonist exposure were measured *in vitro*. These data were integrated by mechanistic modeling, taking into account competitive binding of endogenous dopamine and the antagonist, the turnover of the second messenger cyclic adenosine monophosphate (cAMP), and negative feedback by phosphodiesterase turnover.

Results

The proposed signal transduction model successfully described the cellular cAMP response for 17 D_2 antagonists with widely different binding kinetics. Simulation of the response to fluctuating dopamine concentrations revealed that a significant effect of the target binding kinetics on the dynamics of the signaling only occurs at endogenous dopamine concentration fluctuations with frequencies below 1/min.

Conclusion

Signal transduction and feedback are important determinants of the time course of drug effects. The influence of the D_2 antagonist dissociation rate constant (k_{off}) is limited to the maximal rate of fluctuations in dopamine signaling as determined by the dopamine k_{off} and the cAMP turnover.

Abbreviations: cAMP: cyclic adenosine monophosphate, DMR: Dynamic Mass Redistribution, PDE: Phosphodiesterase, PPHT: poly-3-phenylhydrazone thiophene, RT: room temperature

Introduction

The potential influence of drug-target association and dissociation kinetics on the time course of drug effects (pharmacodynamics) has led to an increasing interest in the use of binding kinetic parameters as a criterion in the selection of drug candidates.[1–6] Although the influence of binding kinetics on the time course of target occupancy has been studied, its exact role in the complex relation between drug dosing and drug effect is potentially complex and not completely understood.[7,8]

Under distinct circumstances, target binding kinetics can influence the pharmacodynamics directly by affecting the time course of the target occupancy. To what extent this occurs depends on values of the rate constants of target association(k_{on}) and dissociation(k_{off}), relative to the pharmacokinetic rate constants characterizing the rates of tissue distribution and elimination. In this regard, additional factors to be taken into consideration are the rate constants characterizing the turnover of the target and the competition with endogenous target ligands. In addition to these direct effects of target binding on the pharmacodynamics, variation in k_{on} and k_{off} can also indirectly influence the pharmacodynamics via signal transduction and homeostatic feedback mechanisms, both at the cellular and the systems level.[7–11] The possible influence of the drug-target dissociation rate constant (k_{off}) on signal transduction has been suggested previously, based on observed *in vitro* efficacy measurements that correlated with k_{off}, but not with the equilibrium dissociation constant K_D.[12,13]

One target for which the influence of drug-target binding kinetics on *in vivo* drug effects is thought to be relevant is the dopamine D_2 receptor. Almost two decades ago, the influence of drug-target binding kinetics on the safety of dopamine D_2 antagonists has been suggested, based on the correlation between low values of k_{off} and the lack of typical side effects, such as extrapyramidal symptoms (i.e. atypicality).[14] This observation led to the hypothesis that quickly dissociating antagonists induce less side effects by allowing displacement from the receptor by fluctuating dopamine concentrations and thus preserving part of the dopamine dynamics, which we will refer to as the "fast-off hypothesis" in this study.[15–18] To understand the influence of dopamine D_2 antagonist binding kinetics on their efficacy and safety, it should be noted that the fluctuations in dopamine concentrations occur at various time scales, ranging from hours to microseconds.[16,19,20] The influence of these target binding kinetics needs to be studied in comparison to dopamine fluctuations at all these time scales.

The dopamine D_2 receptor belongs to the class of inhibitory G-protein coupled receptors (GPCRs). Thus, receptor activation is known to inhibit cAMP production and cAMP in turn is known to stimulate active PDE production, while active PDE stimulates degradation of cAMP. Moreover, GPCR receptor activation can lead to receptor phosphorylation and desensitization as described quantitatively for the β_2-Adrenergic receptor.[21] The production of cAMP is thus regulated by a negative feedback loop, which is a common feature in signal transduction pathways[22].

In this respect, it should be noted that the distinction between agonists and antagonist is often based on historical data and does not always take into account the classification of partial agonists and inverse agonists. One example of this is the study in which Remoxipride was introduced as D_2 antagonist based on its *in vivo* antidopaminergic action and the lack of *in vitro* adenylyl cyclase inhibition in rat striatum homogenate. [23] This study does not report the possibility of adenylyl cyclase stimulation, and inverse agonism is thus not excluded. Moreover, the occurrence of inverse agonism and partial agonism can be influenced by the experimental system and cannot directly be translated across systems. Many D_2 binding drugs that have initially been classified as antagonist have been reported to function as inverse agonists.[24,25] For convenience, we only apply the terms agonist and antagonist in this study, but we assume that the antagonists can have inverse agonistic activities.

In this study, *in vitro* and *in silico* methods were combined to elucidate the influence of D_2 antagonist target binding kinetics on the cellular response to fluctuating dopamine concentrations and to investigate the fast-off hypothesis. Firstly, experimental methods were developed to quantify the binding kinetics of D_2 agonists and antagonists to investigate if the binding kinetics were different for these two types of D_2 ligands.

Secondly, to investigate the fast-off hypothesis with respect to the competition between antagonists and dopamine, the cellular response kinetics after subsequent exposure to dopamine and D_2 receptor antagonists with varying binding kinetics at different levels of the signaling pathway were measured. A minimal mechanistic model combining D_2 receptor binding kinetics, D_2 receptor turnover, cAMP and active PDE turnover was established to describe cAMP concentration *versus* time curves in response to D_2 antagonist exposure. Thirdly, the model was used to identify the role of binding kinetics on drug effect for fluctuating dopamine concentrations. The physiological range of dopamine fluctuation time scales was taken into account by using a frequency response analysis [22,26]. For a more general insight in the influence of binding kinetics on signal transduction, this analysis was expanded to a range of hypothetical turnover rates of cAMP and active PDE.

Methods

This study consists of three parts:

I) *In vitro* measurements of target binding and signal transduction kinetics: drug-target binding parameters of 17 dopamine D_2 antagonists and 12 agonists were measured at room temperature (RT) and at 37°C. Only for the antagonists, the *in vitro* response after dopamine pre-incubation was measured for two different biomarkers: cAMP concentrations over time as second messenger and Dynamic Mass Redistribution (DMR) as a composite signaling marker.

II) Model-based analysis of the *in vitro* cAMP antagonist response curves: A minimal mechanistic model was developed to describe the cAMP responses of the antagonists, based on the target binding kinetics as determined in part I).

III) Frequency Response Analysis: Simulations of the predicted in vivo response to fluctuating dopamine concentrations: The mechanistic model was used to simulate the cAMP response to dopamine concentrations that fluctuate according to a sine-wave pattern with a range of physiologically relevant frequencies between $2 * 10^{-6}$ min^{-1} and 7 min^{-1}. The fluctuation amplitude of cAMP, compared to dopamine, was used to summarize the cAMP response.

I) *In vitro* measurements of target binding and signal transduction kinetics

Equilibrium and Kinetic Probe Competition Assay (ePCA and kPCA)

Affinity and kinetic binding parameters for the 17 studied antagonists and the additional 12 agonists (see Table 1) were measured with a homogeneous time-resolved fluorescence energy transfer (TR-FRET) method as previously described for the Histamine H1 and the GnRH receptors [27,28]. In this study, Tag-lite® Dopamine D_2 labeled cells and a poly-3-phenylhydrazone thiophene (PPHT)-based Dopamine D_2 receptor red antagonist Fluorescent Ligand (both from Cisbio, Codolet, France) were used as receptor-tracer pair to be competed with unlabeled test compounds (Tocris bioscience, TRC, Sigma-Aldrich, Biotrend Chemicals AG or provided by Janssen). Briefly, frozen cells containing the terbium (Tb^{2+}) labeled D_2 receptor, were thawed, spun down and re-suspended in Tag-lite® buffer (Cisbio, Codolet, France) to the concentration indicated by the manufacturer and dispensed into Greiner black small volume 384-well microtiter plates already containing the fluorescent tracer (10 nM end concentration) and the test compounds (antagonists/agonists). These compounds were diluted and transferred to the test plates following the procedures described previously [27].

Starting concentrations of the D_2 antagonist/agonist dilution series were adapted according to their expected affinity, in order to cover a meaningful dose range (see Figure S 1). The ePCA and kPCA experiments as described above were performed at RT and 37°C, for which steady state assay plates were kept in standard tissue culture incubators, whereas for kinetic assays the temperature control function of the PHERAstar FS™ microtiter plate reader was used. For ePCA, tracer and D_2 labeled cells were dispensed to the ready-to-use compound plates to a final volume of 5 µL, and the mixture was incubated for 1-2 h prior to acquisition of the steady state TR-FRET ratiometric signals (665/620 nm) upon excitation at 337 nm. Normalized values were fitted to a logistic 4-parameter model using the Genedata Screener™ software, and

Ki values calculated using the Cheng-Prusoff relationship [29]. For kPCA, the tracer was dispensed to the ready-to-use compound plates prior to introducing them into the PHERAstar FS™ microtiter plate reader. Then the D_2 labeled cells were added to wells to a final volume of 10 µL using the injector system of the instrument, and kinetic TR-FRET readings were made at time zero and every 21-sec or 100-seconds (depending on whether faster or slower compounds were being measured) for the times indicated in Figure S 1. Baseline-normalized kinetic traces were analyzed with a competitive binding kinetics model [30] adapted to deal with normalized- instead of blank-subtracted curves using the Genedata Screener™ software. Prior to D_2 agonist/antagonist testing, binding saturation and kinetic association and dissociation curves for the Dopamine D_2 receptor red antagonist Fluorescent Ligand were recorded as described previously [27,28]. Subsequently, these curves were fitted to the corresponding models using Graph Pad Prism™ in order to obtain the affinity and kinetic constants used as parameters in the Cheng-Prusoff and Motulsky and Mahan models.[29]

cAMP assay

CHO/hD2L and wt-CHO cells were grown in DMEM/F12 with Glutamine (without phenol red, Gibco), 1 % heat inactivated FCS, 1 x Penicillin/ Streptomycin, 400 µg/mL G418. Cells were cultured in humidified atmosphere at 37°C and 5 % CO_2 in air.
To gain insight in the activity of known antagonists after binding to the D2-receptor, changes in the cellular cAMP level were analyzed. To allow real time kinetic measurement, a cAMP-biosensor variant pGloSensor™-22F (Promega Corporation) was used, which consists of a cAMP binding domain (cAMP binding domain B from human PKA regulatory subunit type II β) fused to mutant luciferase. Binding of cAMP results in a conformational change and an increase in luminescence signal. The use of the biosensor system provides a method for a real-time measurement of changes in the cAMP level in a non-lytic assay format. Cells from a Chinese Hamster Ovary (CHO) cell line stably transfected with the long isoform of the human Dopamine 2 receptor, CHO/hD_2L cells, were kindly provided by Janssen Pharmaceutica.

CHO/hD_2L cells (15,000/50 µL) were transiently transfected with the pGloSensor™-22F plasmid (2ng/µL i.a.) using FuGeneHD transfection reagent (3 µL FuGeneHD: 1 µg DNA plasmid, Promega, Madison, USA). By reaching 70-80% confluency, cells were harvested using Trypsin/EDTA and resuspended in DMEM/F-12/ HEPES medium supplemented with 1% fetal calf serum (FCS), Pen/Strep and 1 mg/ml G418. Prior to addition of the pGloSensor™-22F plasmid to cells, it was incubated for 20 min with the FuGeneHD transfection reagent at room temperature. By the end of incubation time, the cells and transfection solution were combined, mixed and plated in white, solid bottom 384 well assay plates (Greiner CELLSTAR® 384 well plates). After 24 h of incubation the transfection mixture was replaced by 20 µL/well DMEM/F-12/HEPES medium with 9% Glo-substrate followed by 2 h incubation at room temperature. To achieve a good signal window, CHO/hD_2L cells were treated with 3 µM forskolin for 30 min. Forskolin was used as an activator of the adenylate cyclase and therefore for a receptor-independent increase of the cellular cAMP level. In order to monitor antagonist activity against the natural receptor ligand, cells were incubated with 15 nM dopamine for 20 min prior to addition of antagonists. D_2 receptor antagonists were tested in a 10-point dose response (top concentration 10 µM, 1:4 dilutions). Signal kinetics was detected for a total period of 1h every 2min. All compounds were dissolved in dimethyl sulfoxide (Carl Roth GmbH + Co. K, Karlsruhe, Germany).

Dynamic mass redistribution (DMR) Assay

For DMR measurements[31], 10 µl/ well cell culture media(DMEM/ F12 without phenol red, Gibco) were transferred into an EnSpire-LFC 384– fibronectin coated plate (PerkinElmer, Waltham, USA) and incubated for 30 min. A suspension of CHO/hD_2L cells in cell culture media was prepared and cells were seeded into the label-free cellular (LFC) plate (1.5 x 10^4 cells/well), resulting in a final volume of 30 µl/ well. The LFC plate was incubated overnight in a humidified atmosphere at 37°C and 5 % CO2 in air.
On the next day, label-free assay buffer (HBSS (Sigma Aldrich), 20 mM HEPES (Sigma Aldrich), 0.5 % (v/v) DMSO, 0.05 % v/v Pluronic (AnaSpec)) was prepared. Dopamine was diluted in label-free assay buffer (5 uM, final assay concentration) and dispensed into an intermediate plate (Polypropylen 384 well microplate

(Greiner Bio-One GmbH, Frickenhausen, Germany)). Of each antagonist, a dilution series in dimethyl sulfoxide was prepared and transferred into an intermediate plate. Label free assay buffer was added to the intermediate plate to dilute the antagonists further.
The media was removed from the LFC plate by washing the wells four times with label-free assay buffer (25 µl/ well). The total assay volume after the washing step was 30 µl/ well. The LFC plate was placed in an EnSpire multimode reader equipped with Corning® Epic® Label-free technology (PerkinElmer). After 2 h, a baseline was recorded (10 minutes) followed by the addition of Dopamine or vehicle control (10 µl/well) from the intermediate plate. Antagonist dispensing and mixing was automated using a Janus Workstation (PerkinElmer). A 20-min kinetic DMR measurement was recorded on the EnSpire multimode reader. Directly afterwards, the D_2R antagonists were transferred from the intermediate plate to the LFC plate (10 µl/well) and a 90-min kinetic DMR measurement was initiated on the EnSpire multimode reader.

II) Model-based analysis of the *in vitro* cAMP antagonist response curves

Modeling procedure

To obtain a detectable cAMP signal, adenylyl cyclase was activated first by forskolin. The dynamics of this activation was recorded in a separate experiment. Since the cAMP response to forskolin addition was measured separately from the cAMP response to the D_2 receptor antagonists, the D_2 antagonist response measurements were normalized to the average cAMP response before antagonist addition (baseline). A mechanistic model, based on previous models and mechanistic information from literature [21,24,25,32–34], combining dopamine-receptor binding kinetics, antagonist-receptor binding kinetics, and cAMP as well as active PDE turnover to describe the generation of the cAMP response was used to simultaneously fit the cAMP data of all compounds. A diversity of models, with differences in mechanistic detail (Table 2), was tested for their utility to describe the cAMP responses. Model fitting was performed in NONMEM v7.3 using ADVAN9. All values of k_{off}, including the k_{off} of dopamine, were fixed to the values that were measured according to the methods described above, while the K_D values were estimated. Models were selected based on the objective function value (OFV) and visual inspection of the individual fits of the experiments. A schematic overview of the final model structure that was fitted to the cAMP response data (model 1) is given in Figure 1.

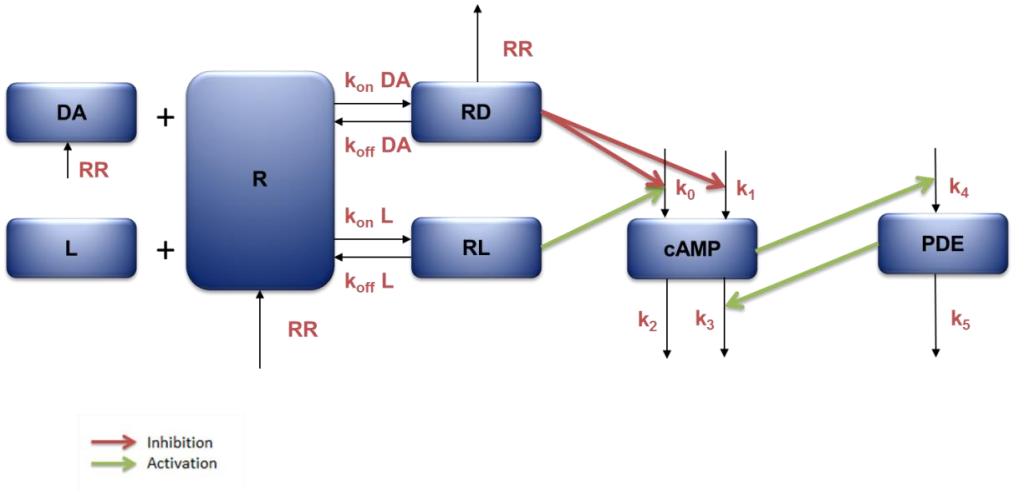

Figure 1. Schematic overview of the structure of the final model (Model 1). DA denotes dopamine, L denotes the antagonist, R denotes the D_2 receptor RD the D_2 receptor-dopamine complex, RL the receptor antagonist complex. RR indicates receptor recycling; the internalization (or degradation) of the dopamine-receptor complex and the resurfacing (or synthesis) of the unbound receptor and dopamine. Black arrows denote mass transfer, green arrows an activating interaction, red arrows an inhibiting interaction. The equations of Model 1 are given in Supplement S 3.

III) Frequency Response Analysis: Simulations of the predicted *in vivo* response to fluctuating dopamine concentrations

Dopamine concentrations were varied over time according to a sine wave with various frequencies and an amplitude of 10 nM. This dopamine fluctuation induces fluctuations in the cAMP concentrations, but the amplitude of these fluctuations is dependent on the frequency of the dopamine fluctuations. To get a complete analysis of the cAMP response to fluctuating dopamine concentrations in the presence of an antagonist and to cover all physiologically relevant frequencies [16,19,20], a wide frequency range was tested between 2 * 10^{-6} min^{-1} and 7 min^{-1}. After the cAMP concentration had reached constant fluctuation around the average steady state (i.e. the mean of the minimal and maximal concentration), the amplitudes of both the dopamine and the cAMP concentrations were converted amplitudes relative to their average steady state values and their ratio was defined as the "cAMP gain", according to equation 1. This gain is a measure for the degree in which dopamine fluctuations results in cAMP fluctuations. All simulations were performed in Rstudio using the deSolve package and the lsoda differential equation solving method.[35,36]

$$Gain\ cAMP = \frac{\frac{amplitude\ cAMP}{average\ steady\ state\ cAMP}}{\frac{amplitude\ dopamine}{average\ steady\ state\ dopamine}} \qquad \text{Eq. 1}$$

Results

I) *In vitro* measurements of target binding and signal transduction kinetics

We have used a novel TR-FRET based assay technology to measure the K_D, k_{on} and k_{off} values of 17 dopamine D_2 antagonists and 12 agonists at both room temperature and 37°C. The results (shown in Figure 2, Table 1, Table S 1 and Table S 2) are in good agreement with previous literature reports that used radioligand binding [17,18,37–46]. Figure 2 shows that both the D_2 antagonists and agonists in this study had diverse combinations of k_{on} and k_{off} values, and that none of them had a combined low k_{on} and low k_{off} value. Figure 2 also shows that the investigated agonists tend to have higher k_{off} values and lower k_{on} values compared to the investigated antagonists. For compounds with higher dissociation rates than the competing fluorescent ligand (k_{off} ≥ 0.01 s^{-1}) the precision of their k_{off} estimates is limited, or only the lower limit could be identified. However, for the experiments and model fits in this study, the exact value of the k_{off} has less influence on the cAMP concentration for fast compared to slow dissociating compounds and a low precision for high k_{off} values is thus acceptable for the scope of this study.

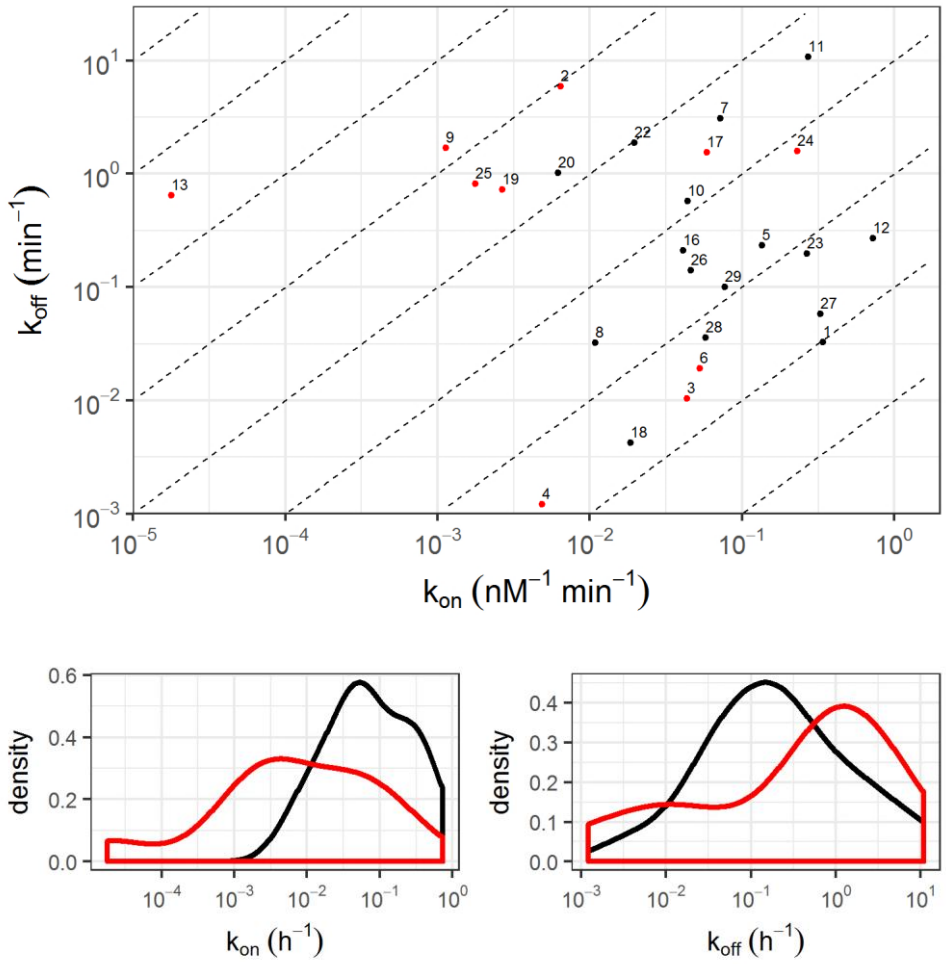

Figure 2. In vitro measurements of k_{on} and k_{off} for each of the measured D_2 antagonists from the kPCA assay at room temperature. Red symbols/lines represent agonists, black symbols/lines antagonists. Upper panel: The numbers refer to the compound numbers in Table 1. Lower panel: distribution of k_{on} and k_{off} for agonists compared to antagonists, plotted as the estimated probability density function.

Table 1. *In vitro* measurement of k_{on}, k_{off}, their standard deviation (SD) and the calculated K_D for each of the measured D_2 antagonists from the kPCA assay at room temperature. NA: not available, NPA: N-n-Propyl Apomorphine

Compound ID	#	K_D [M]	SD	k_{on} [1/(M*s)]	SD	k_{off} [1/s]	SD
(-)-Nemonapride	1	9.58E-11	3.26E-12	5.66E+06	2.73E+05	5.43E-04	4.46E-05
(-)-Quinpirole	2	7.80E-07	6.28E-07	1.07E+05	4.77E+04	9.82E-02	1.04E-01
Aripiprazole	3	2.39E-10	4.40E-13	7.24E+05	3.17E+05	1.73E-04	7.52E-05
Bromocriptine	45	2.19E-10	1.96E-10	8.09E+04	2.54E+04	2.02E-05	1.80E-05
Bromperidol	5	1.89E-09	7.49E-10	2.26E+06	9.57E+05	3.91E-03	1.21E-04
Cabergoline	6	4.26E-10	2.13E-10	8.80E+05	5.13E+05	3.21E-04	3.15E-05
Clozapine	7	5.05E-08	1.28E-08	1.20E+06	1.44E+06	5.13E-02	5.74E-02
Domperidone	8	3.04E-09	5.08E-10	1.81E+05	5.26E+04	5.37E-04	6.75E-05
Dopamine	9	1.27E-06	5.56E-07	1.88E+04	2.16E+04	2.82E-02	3.01E-02
JNJ-37822681	10	9.32E-09	2.71E-09	7.33E+05	NA	9.54E-03	NA
JNJ-39269646	11	4.87E-08	8.35E-09	4.53E+06	4.51E+06	1.79E-01	1.64E-01
Haloperidol	12	3.82E-10	4.98E-11	1.21E+07	5.18E+06	4.48E-03	1.37E-03
Memantine	13	2.61E-05	9.91E-06	2.98E+02	NA	1.07E-02	NA
NPA	14	NA	NA	NA	NA	NA	NA
Olanzapine	15	8.58E-09	3.38E-09	> 7.30E+05	NA	> 1.00E-02	NA
Paliperidone	16	5.45E-09	2.07E-09	6.81E+05	1.83E+05	3.52E-03	4.14E-04
Pergolide	17	2.44E-08	1.24E-08	9.81E+05	NA	2.59E-02	NA
Pimozide	18	2.55E-10	6.74E-11	3.10E+05	2.45E+05	7.08E-05	4.17E-05
Piribedil	19	2.23E-07	5.90E-08	4.43E+04	9.30E+03	1.21E-02	4.18E-03
Quetiapine	20	1.50E-07	6.94E-08	1.03E+05	2.04E+04	1.69E-02	6.07E-03
R-(-)-Apomorphine	21	1.70E-07	7.68E-08	> 8.85E+04	NA	> 1.00E-02	NA
Remoxipride	22	8.31E-08	3.47E-08	3.28E+05	NA	3.14E-02	NA
Risperidone	23	7.56E-10	7.62E-11	4.43E+06	8.54E+05	3.31E-03	3.09E-04
Rotigotine	24	7.82E-09	2.86E-09	3.84E+06	3.78E+06	2.65E-02	2.75E-02
S-(+)-Apomorphine	25	3.33E-07	1.15E-07	2.94E+04	NA	1.36E-02	NA
Sertindole	26	4.07E-09	2.23E-09	7.70E+05	7.00E+05	2.35E-03	1.13E-03
Spiperone	27	1.79E-10	4.11E-12	5.44E+06	1.11E+06	9.70E-04	1.76E-04
S-(+)-Raclopride	28	6.34E-10	1.15E-10	9.57E+05	1.81E+05	5.96E-04	4.62E-06
Ziprasidone	29	1.31E-09	8.40E-11	1.29E+06	2.01E+05	1.67E-03	1.55E-04

Our cAMP and DMR measurement provide a new and extensive set of signal transduction data for 17 D_2 antagonists. Figure 3 shows the measured cAMP concentrations during the complete time course of a typical experiment with and a control experiment without dopamine D_2 receptor transfection. For comparison, the DMR responses are given in Supplement S 2, Figure S 3. In Figure 4, the complete set of measured cAMP time courses for all 17 D_2 antagonists at 10 different concentrations is given, together with their model fits. The data in Figure 4 show that the antagonists with lower k_{off} values (pimozide, domperidone, raclopride) induce cAMP concentration-time curves for the lower antagonist concentrations, with later and lower peak concentrations, compared to faster dissociating compounds (JNJ-39269646, Clozapine, Olanzapine). However, this trend was not observed in the DMR data (see Supplement S 2).

II) Model-based analysis of the *in vitro* cAMP antagonist response curves

Model selection

A series of related model structures, which differed in mechanistic detail, was evaluated for their utility to describe the cAMP responses (Table 2). From these models, Model 1 was selected as the final model for further analyses. This model selection was based on the lowest Objective Function Value (OFV) and on the goodness of fit, as described in the methods. In Model 1, all antagonists also functioned as inverse agonists by stimulating cAMP production (see Figure 1), and the inverse agonism efficacy was estimated by the model for each antagonist. Model 1 was compared with alternative models to ensure that Model 1 was the optimal model:

Model 2 incorporated more mechanistic detail compared to Model 1 by including the role of PKA in linking the cAMP concentrations to active PDE concentrations. The performance of Model 2 was identical to the

performance of the simpler Model 1. In addition, the estimated value of PKA turnover was high compared to cAMP and active PDE turnover, which means that the PKA addition to the model did not introduce any further delay in the response kinetics.
Models 3 and 4 were simplified models compared to Model 1 that excluded inverse agonism and receptor recycling, respectively. Model 3 and 4 clearly performed worse than Model 1, as indicated by the much higher OFVs.
Model 5 included dopamine elimination/degradation, but this did not improve the model fit.
Model 6 used a fixed value for k_5 which was set to 0. This model performed slightly better than Model 1. The value of k_5 (0.0005 min^{-1}) in the final model (Model 1) was chosen for a combination of physiological and numerical reasons: setting k_5 to zero as in Model 6 would mean that active PDE is only synthesized and not degraded, which would result in a physiologically implausible infinite increase in active PDE concentrations. Moreover, all other parameter values than k_5 differed maximally 5% between Model 6 and Model 1.
Finally, Model 7 demonstrates the contribution of slow binding kinetics to the model fit of the final model, as the exclusion of slow binding kinetics (k_{off} was set to 10 min^{-1} for all antagonists in Model 7) resulted in a large increase of the OFV, compared to Model 1.

Table 2. Overview of the Objective Function Values (OFVs) of the final model and the tested alternative models. The changes compared to Model 1 are indicated by the mechanistic detail that was added (+) or removed (-) from Model 1.

#	Model	OFV	model fit
1	Final model	62404	successful
2	+ PKA	62411	successful
3	- inverse agonism (k0)	102215	terminated
4	- receptor recycling (RR)	81594	terminated
5	+ degradation of dopamine	62404	successful
6	- active PDE degradation (k_5)	62307	successful
7	+ assumption of fast binding kinetics	67468	successful

Model fitting

The model fits of Model 1 in Figure 4 demonstrate that the general shape of the cAMP concentration-time curve and the concentration-dependency of the antagonist effect on the cAMP concentration are well captured by the model for all compounds. The equations of Model 1 are given in Supplement S 3. For a few compounds (i.e. Clozapine, Bromperidol) the peak cAMP concentration or the cAMP concentrations in the terminal phase for the highest antagonist concentrations are underpredicted. The parameter estimates that were the same for all antagonists are given in Table 3 and all parameter estimates are given in Supplement S 3, Table S 3. The uncertainty in the parameter estimates is low, as indicated by the small residual standard errors.

Table 3. Estimates for the system-specific parameters and their uncertainties from fitting Model 1 to the cAMP response data. Naming of the parameters corresponds to Figure 1. $DAFR_{50}$ denotes the ratio of the total receptor concentration divided by the dopamine-bound receptor concentration that inhibits the maximal cAMP synthesis to 50%, R_{tot} denotes the total receptor concentration, k_{0max} denotes the maximal value of k_0. h denotes the hill factor of the non-linear relationship between D_2 receptor occupancy and cAMP synthesis (k_0). The dopamine k_{off} was based on the *in vitro* measurements and the chosen values for k_4 and k_5 are described in the text. RSE: Relative Standard Error.

Parameter	Value (unit)	RSE (%)
K_D dopamine	10.3 (nM)	4.0
k_{off} dopamine	1.69 (min^{-1})	Input parameter
$DAFR_{50}$	2.25	2.4
R_{tot}	1.74 (nM)	1.3
RR	0.238 (min^{-1})	2.2
k_{0max}	20.5 ($AU \cdot min^{-1}$)	0.50
k_1	4.12 ($AU \cdot min^{-1}$)	0.80
k_2 (active PDE-independent)	0.0334 (min^{-1})	11
k_3 (active PDE-dependent)	0.00882 ($nM^{-1} \cdot min^{-1}$)	0.20
k_4	0.00882 (min^{-1})	defined as identical to k_3
k_5	0.0005 (min^{-1})	input parameter
h	1.77	0.40

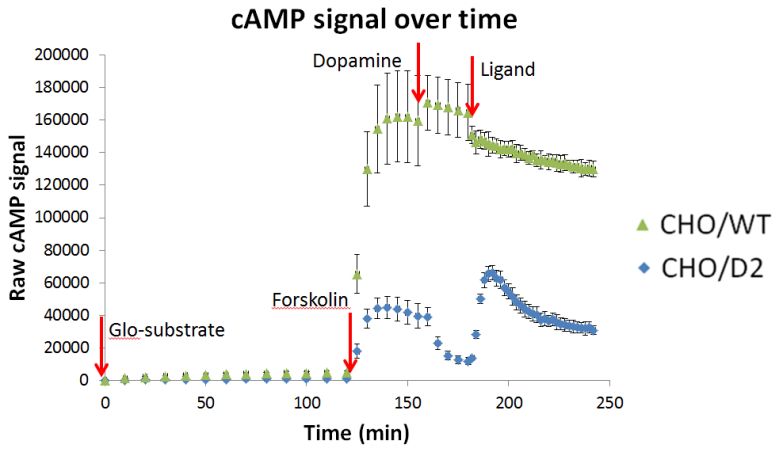

Figure 3. Measured cAMP response during a typical experiment of the cAMP assay (see Methods). The arrows indicate addition of Glo-substrate, Forskolin, Dopamine and the tested ligand. The light grey data points were measured in wild type CHO cells, while the dark grey data points were measured in CHO cells transfected with the dopamine D2 receptor.

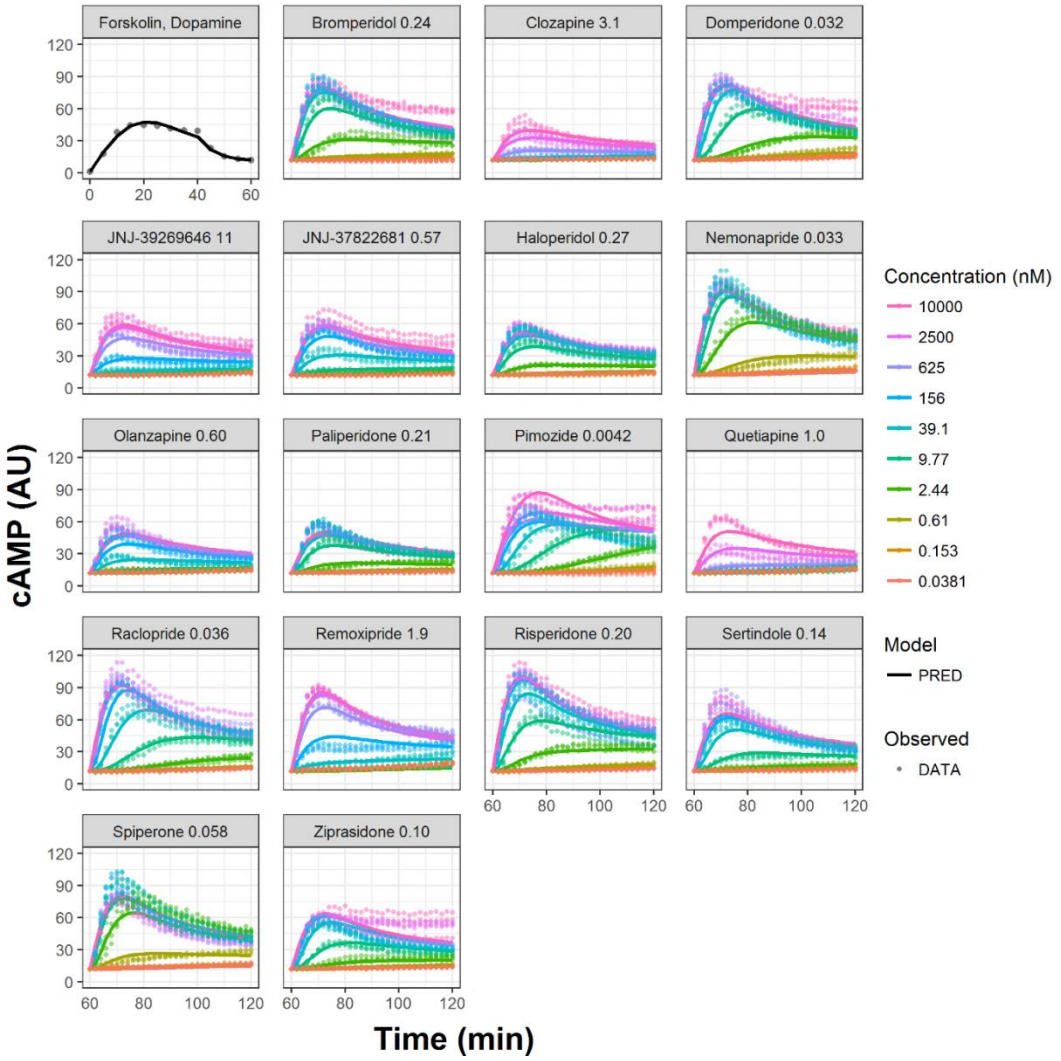

Figure 4. Model fits for all in vitro cAMP data as measured in transfected CHO cells. Both the observed (dots) and model-predicted (lines) cAMP signals are included. The order of the lines and symbols correspond to the order of the concentrations in the legend. The top-left panel shows the cAMP measurements and model predictions for the first 60 minutes in between forskolin addition and antagonist addition. The lower panels only show the time points after antagonist addition.

III) Frequency Response Analysis: Simulations of the predicted in vivo response to fluctuating dopamine concentrations

The simulations of the response to fluctuating dopamine concentrations resulted in a fluctuation pattern of cAMP over time for each dopamine fluctuation frequency that was tested. The cAMP fluctuation amplitude was dependent on the frequency, as illustrated in Figure 5.

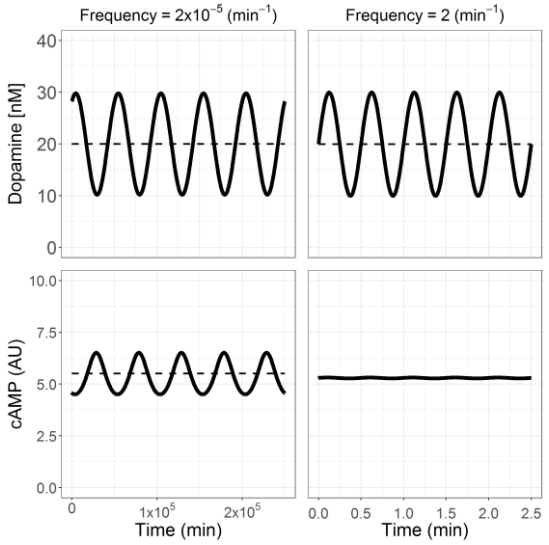

Figure 5. Example simulations of fluctuations in dopamine concentration for a low frequency (left-hand plots) and a high frequency (right-hand plots). The dashed lines indicate the average steady state values of the fluctuations, which is calculated as the mean of the maximal and the minimal concentration. Note the different time scales on the left compared to the right plots. The antagonist k_{off} was 2.5 min^{-1} for these simulations.

From these dopamine and cAMP fluctuations, the relative amplitudes and the ratio of these relative amplitudes could be calculated to obtain the cAMP gain (Equation 1, see Methods) as illustrated in Figure 6. The two simulations in Figure 5 and Figure 6 thus provide two points on the line for an antagonist k_{off} of 2.5 min^{-1} in the graph of Figure 7; at a frequency of 2 x 10^{-5} min^{-1} and 2 min^{-1}, the cAMP gain is 0.36 and 0.0080, respectively.

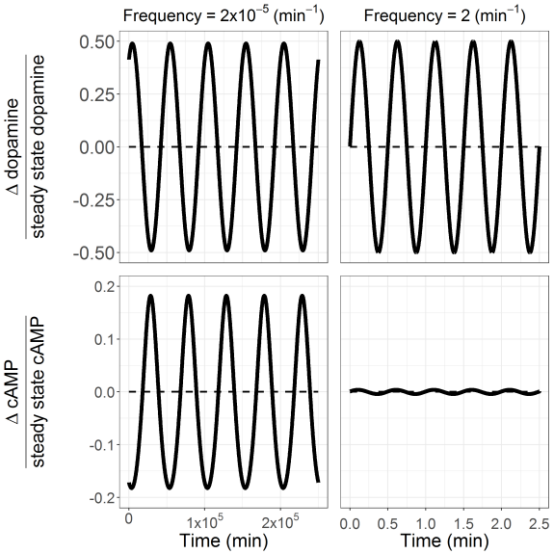

Figure 6. Converted dopamine and cAMP concentrations into relative fluctuations compared to average steady state. The delta sign refers to the difference between the concentration and the average steady state concentration. From this data, the gain can be identified according to equation 1, which is approximately 0.36 for the left-hand plots and 0.0080 for the right-hand plots. The antagonist k_{off} was 2.5 min^{-1} for these simulations.

From the Frequency Response Analysis as shown in Figure 7, the following was observed:

If dopamine fluctuations occur slowly, the cAMP response has a steady gain (i.e. the cAMP fluctuations have a constant amplitude) for frequencies lower than $1*10^{-5}$ min^{-1} in Figure 7. This gain is increased for intermediate frequencies (between $1*10^{-4}$ and 0.1/min) and decreases steeply for higher frequencies. The influence of drug-target binding kinetics on the transduction of dopamine fluctuations into cAMP fluctuations is limited to intermediate frequencies between $1*10^{-4}$ and 0.1/min of dopamine fluctuations.

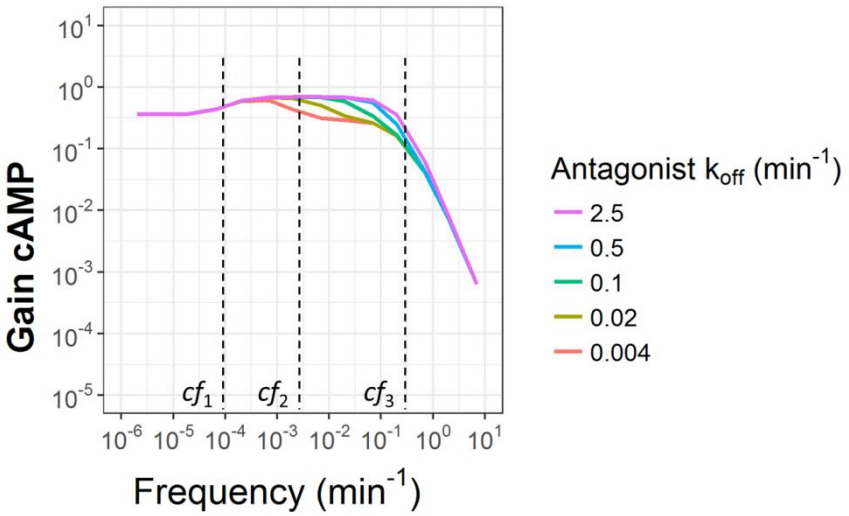

Figure 7. Frequency response analysis of the relative amplitude of cAMP fluctuations normalized to the relative amplitude of dopamine fluctuations (gain). The frequency on the x-axes denotes the frequency of the dopamine concentration sine wave that has been used as input for the simulations. The different colors represent different dissociation rate constants (k_{off}) for the antagonist. The applied antagonist concentration was 14 nM while the antagonist K_D was 6.9 nM for all simulations in both plots. The applied dopamine concentrations had a median value of 20 nM and an amplitude of 10 nM. The value of k_{on} changed simultaneously with k_{off} such that the K_D was constant. The dashed lines indicate characteristic frequencies for the line where k_{off} = 0.004 min^{-1} at which the gain increases (cf_1) and decreases (cf_2) to new plateau values and decreases linearly with increasing frequencies (cf_3). The order of the lines follows the order of the legend.

The model-based frequency response analysis allowed characterization of the cAMP response to a wide range of dopamine fluctuation frequencies (as shown in Figure 7). This analysis identified the influence of each model parameter on the cAMP response. The cAMP gain versus dopamine fluctuation frequency graphs as shown in Figure 7 are dependent on the antagonist k_{off} and can have up to three characteristic frequencies around which the gain changes. The positions of the characteristic frequencies are dependent on the parameter values, as discussed below, and have been derived empirically from the gain *versus* frequency plot as the frequencies at which the cAMP gain starts to change. These frequencies were numbered cf_1, cf_2, and cf_3, as indicated in Figure 7. From the lowest dopamine fluctuation frequencies to cf_1, the cAMP gain is independent of the antagonist k_{off} and does not change with increasing frequency, until cf_1 is reached where the gain increases towards a new plateau value. The frequency at which the cAMP gain declines to a new plateau value, cf_2, is dependent on the antagonist k_{off} and cannot be observed for high-k_{off} antagonists, which is the case for k_{off} values between 0.5 and 2.5 min^{-1} (Figure 7). The third characteristic frequency, cf_3, is independent of the antagonist k_{off} and introduces a decline in the cAMP gain that is linear with the increasing frequency.

The influence of the model parameters on the characteristic frequencies was identified by repeating the FRA for different values of each model parameter, as shown in Supplement S 5. As illustrated by Figure S 5, the value of cf_1 depends on the value of the active PDE turnover rate constant k_5. This can be understood by

considering that the increase in cAMP gain is caused by a reduced negative feedback if the turnover of active PDE is to slow, relative to the fast fluctuations of cAMP. The second characteristic frequency, cf_2, is influenced by the antagonist k_{off} and by the antagonist concentration, as illustrated in Figure S 8. The role of the antagonist k_{off} can be explained by the slow displacement of antagonists with a low k_{off} value and the consequently reduced fluctuation of dopamine receptor occupancy. The role of the antagonist concentration can be explained by the higher antagonist receptor occupancy and the relatively lower influence of fluctuating dopamine concentrations on the antagonist receptor occupancy for higher antagonist concentrations. The third characteristic frequency, cf_3, is determined by both the cAMP turnover and the dopamine k_{off}, as shown in Figure S 6 and Figure S 7, respectively. These parameters determine the turnover of cAMP and dopamine receptor occupancy, respectively, and the slowest turnover is thus rate-limiting for the eventual turnover of cAMP and the maximal frequency of dopamine fluctuations that can be translated into cAMP fluctuations without a declining fluctuation amplitude. In summary, if k_5 (active PDE turnover) increases, cf_1 increases, if the antagonist concentration or k_{off} increases, cf_2 increases and if k_3 (cAMP turnover) increases, cf_3 increases

Overall, the translation of fluctuating dopamine concentrations into fluctuation of cAMP concentrations is inhibited to a larger extent by antagonists with a low k_{off} value compared to antagonists with a high k_{off} value. However, this role of the antagonist k_{off} is only present if the dopamine fluctuation frequency is not too high (i.e. higher than cf_3) to be translated and not too slow (i.e. lower than cf_2) to be able to displace even a slow dissociating antagonist.

Discussion

In this study, we developed a minimal mechanistic model that describes the cellular effects of dopamine D_2 antagonism on cAMP turnover, including both dopamine and antagonist receptor binding kinetics as well as active PDE turnover. The model was able to describe successfully *in vitro* binding and cAMP concentration-time profiles data obtained for 17 D2 antagonists. Compared to fast dissociating antagonists, slowly dissociating D_2 antagonists lead to a reduced response to fluctuating dopamine concentrations as previously suggested in the fast-off hypothesis (see below) for dopamine antagonists. However, this influence of antagonist binding kinetics is only observed when the dopamine fluctuations have a frequency in the range of 1/min to 1/hour. This range is determined by the cAMP turnover, the dopamine k_{off} and the antagonist k_{off}.

Insight into the influence of target binding kinetics on dopamine D_2 antagonism

According to the fast-off hypothesis for dopamine D_2 antagonists, it is beneficial if dopamine can displace D2 antagonists receptor binding, to avoid extrapyramidal side effects.[15] Since the dopamine fast-off hypothesis only applies to D_2 antagonists, one would expect more antagonists with a high k_{off} value, compared to agonists, for which a high k_{off} value is not considered beneficial. However, our results in Figure 2 show that the k_{off} of agonists tends to be higher compared to antagonists. The k_{off} values that would be necessary for the displacement of dopamine according to the fast-off hypothesis were analyzed previously, [16] but the kinetics of signal transduction were not taken into account in that study. Here we show that the displacement of D_2 antagonists by dopamine is not generating a fluctuating response if the frequency of fluctuation in dopamine D_2 occupancy is higher than what the endogenous signal transduction can translate into a cellular signal, such as cAMP fluctuation. In this study, it is indicated that the rate of endogenous signal transduction is limited both by the dopamine k_{off} and by the cAMP turnover. It was found that D_2 antagonists that dissociate faster than haloperidol (a typical antipsychotic) will lead to a similar signal transduction of fluctuating dopamine concentrations as haloperidol. However, this is in conflict with the fast-off hypothesis.[15] Moreover, this fast-off hypothesis has been challenged recently by *in vitro* electrophysiology measurements that revealed only moderate differences (6.4-2.5 fold) in recovery rates of the electrophysiological response to dopamine in oocytes between atypical antagonists and the typical antagonist haloperidol [47].

Extrapolation of *in vitro* to *in vivo* antagonism and signal transduction

Our analysis demonstrates that the fast-off hypothesis for D_2 antagonists is only relevant for a limited range of antagonist k_{off} values and not applicable to sub-second pulses of dopamine release in the synaptic cleft. Moreover, this study reveals how the relevance of the D_2 antagonist k_{off} depends on the kinetics of signal transduction and negative feedback. Although we provide a quantitative estimate of the maximal value of k_{off} that could decrease the inhibited transduction of dopamine fluctuations, it should be noted that this value cannot be translated directly into the *in vivo* situation.

Firstly, the temperature at which the signal transduction experiments were performed, room temperature, is not the physiological temperature, and most reactions (including drug-target binding kinetics) will be faster at 37°C. However, the difference in binding kinetics between these temperatures is moderate, although highly variable: the ratio of the k_{off} values for the measured D_2 antagonists in this study at 37°C divided by the k_{off} at room temperature was 3.2 fold on average and between 0.10 and 7.4 in the whole dataset, while for k_{on} this ratio was 2.5 on average and between 0.038 and 6.7 (see Supplement S 1). Therefore, we expect that the kinetics of signal transduction will be different at 37°C compared to our measurements at room temperature, but we do not expect differences of more than one order of magnitude.

Secondly, the analysis of Model 1 in this study only incorporates signal transduction into cAMP and active PDE levels, while in the clinical *in vivo* situation, more transduction steps are involved before the antipsychotic effect of D_2 antagonists is obtained. The differences between the time curves of cAMP and cellular optical density as measured by DMR (Supplement S 2), provide a first indication of possible differences between the cAMP response and downstream signaling, but the mechanistic interpretation of cellular optical density requires more advanced experimental designs.[48]

Thirdly, the analysis of the cAMP response data with Model 1-7 is not sufficient to obtain a conclusive and comprehensive description of the mechanism(s) underlying the observed cAMP responses. Although various mechanisms were represented by Model 1-7 and fitted to the data, some of these models provide similar fits (e.g. Model 1 and Model 5) and the true mechanism cannot be identified based on these fits alone. Also, the transfected CHO cells used in the in vitro measurements of CAMP are not brain cells, and the system-specific parameter values as obtained by the model fit in this study might therefore be different from the in vivo situation.

All of these factors might explain why the receptor recycling rate constant as identified here (0.238 min^{-1}) does not correspond to previous more direct estimates of the D_2 receptor degradation rate constant from rat striatum (0.0001 min^{-1})[49,50]. However, the critical elements in the structure of Model 1 are well supported by previous studies: Inverse agonism has been reported for many of the D_2 antagonists as described in the introduction [24,25]. The active PDE-independent degradation of cAMP has been described before in a more extensive GPCR signaling model [21] and is also supported by the different molecules that can hydrolyze cAMP [33,34]. The two cAMP production rate constants represent the constitutive receptor activity, which is inhibited by inverse agonism [32], and the remaining cAMP production.

Finally, the frequency response analysis that was used here is based on a sine-wave function while the dopamine fluctuations in the brain occur with a more variable frequency and amplitude.[16,19].

Although the absolute limit of the influence of binding kinetics on antagonist effects cannot be translated directly into the *in vivo* situation, our findings demonstrate that such a limitation likely exists in the *in vivo* situation as well, and may be expected to be in the order of minutes. These results make it highly unlikely that sub-second dopamine fluctuations can be translated into cAMP fluctuations and that sub-second k_{off} values are required to minimize extrapyramidal side effects. This also indicated that it is highly unlikely that antagonists with sub-second dissociation half-lives yield different inhibition of dopamine signaling compared to antagonists with dissociation half-lives in the second-minute range, as suggested before.[16]

We have shown that for a common transduction system including an indirect effect and a negative feedback loop, the relevance of fast drug-target dissociation is limited by the target dissociation of the endogenous ligand and the turnover of the second messenger. The rate constants for dopamine dissociation from the D_2 receptor and cAMP turnover that we have obtained in this study challenge the fast-off hypothesis. Our study demonstrates that the influence of target binding kinetics on drug effects cannot be fully understood without taking into account signal transduction and feedback kinetics, especially if fluctuating endogenous ligand concentrations are present.

Conclusion

The cellular cAMP response to dopamine D_2 antagonists could be described using a minimal mechanistic model including *in vitro* measured dopamine and antagonist D_2 binding kinetics, in conjunction with synthesis and degradation of cAMP and active PDE. This model revealed that slowly dissociating D_2 antagonists show a reduced transduction of dopamine fluctuations into cAMP fluctuations, compared to fast dissociating antagonists. However, this influence of the dissociation rate constant is limited to dopamine fluctuations that are faster than the k_{off} value of the drug but slower than the dopamine k_{off} value and the cAMP turnover. In general, we conclude that the influence of drug-target binding kinetics on drug effect kinetics is dependent on the dynamics of signal transduction kinetics and that both the turnover of second messengers and the k_{off} value of endogenous ligands limit the discrimination between fast and slowly dissociating antagonists.

Acknowledgements

This research is part of the K4DD (Kinetics for Drug Discovery) consortium which is supported by the Innovative Medicines Initiative Joint Undertaking (IMI JU) under grant agreement no. 115366. The IMI JU is a project supported by the European Union's Seventh Framework Programme (FP7/2007–2013) and the European Federation of Pharmaceutical Industries and Associations (EFPIA).

References

1. Copeland RA, Pompliano DL, Meek TD. Drug-target residence time and its implications for lead optimization. Nat Rev Drug Discov 2006;5(9):730–9
2. Zhang R, Monsma F. Binding kinetics and mechanism of action: toward the discovery and development of better and best in class drugs. Expert Opin Drug Discov 2010;5(11):1023–9
3. Lu H, Tonge PJ. Drug-Target Residence Time: Critical Information for Lead Optimization. Curr Opin Chem Biol 2011;14(4):467–74
4. Dahl G, Akerud T. Pharmacokinetics and the drug-target residence time concept. Drug Discov Today 2013;18(15–16):697–707
5. Vauquelin G. Impact of target binding kinetics on in vivo drug efficacy: k off , k on and rebinding. Br J Pharmacol 2016;173(15):2319–34
6. Copeland RA. The drug-target residence time model: a 10-year retrospective. Nat Rev Drug Discov 2016;15(2):87–95
7. de Witte WEA, Wong YC, Nederpelt I, et al. Mechanistic models enable the rational use of in vitro drug-target binding kinetics for better drug effects in patients. Expert Opin Drug Discov 2016;11(1):45–63
8. Yin N, Pei J, Lai L. A comprehensive analysis of the influence of drug binding kinetics on drug action at molecular and systems levels. Mol Biosyst 2013;9(6):1381–9
9. Landersdorfer CB, He Y-L, Jusko WJ. Mechanism-based population modelling of the effects of vildagliptin on GLP-1, glucose and insulin in patients with type 2 diabetes. Br J Clin Pharmacol 2012;73(3):373–90
10. Kleinbloesem CH, van Brummelen P, Danhof M, et al. Rate of increase in the plasma concentration of nifedipine as a major determinant of its hemodynamic effects in humans. Clin Pharmacol Ther 1987;41(1):26–30
11. Francheteau P, Steimer JL, Merdjan H, et al. A mathematical model for dynamics of cardiovascular drug action: Application to intravenous dihydropyridines in healthy volunteers. J Pharmacokinet Biopharm 1993;21(5):489–514
12. Guo D, Mulder-Krieger T, IJzerman AP, et al. Functional efficacy of adenosine A_2A receptor agonists is positively correlated to their receptor residence time. Br J Pharmacol 2012;166(6):1846–59
13. Sykes DA, Dowling MR, Charlton SJ. Exploring the mechanism of agonist efficacy: a relationship between efficacy and agonist dissociation rate at the muscarinic M3 receptor. Mol Pharmacol 2009;76(3):543–51
14. Meltzer HY. What's atypical about atypical antipsychotic drugs? Curr Opin Pharmacol 2004;4(1):53–7
15. Kapur S, Seeman P. Does Fast Dissociation From the Dopamine D 2 Receptor Explain the Action of Atypical Antipsychotics ?: A New Hypothesis. Am J Psychiatry 2001;158(3):360–9
16. Vauquelin G, Bostoen S, Vanderheyden P, et al. Clozapine, atypical antipsychotics, and the benefits of fast-off D2 dopamine receptor antagonism. Naunyn Schmiedebergs Arch Pharmacol 2012;385(4):337–72
17. Langlois X, Megens A, Lavreysen H, et al. Pharmacology of JNJ-37822681, a specific and fast-dissociating D2 antagonist for the treatment of schizophrenia. J Pharmacol Exp Ther 2012;342(1):91–105
18. Kapur S, Seeman P. Antipsychotic agents differ in how fast they come off the dopamine D2 receptors. Implications for atypical antipsychotic action. J Psychiatry Neurosci 2000;25(2):161–6
19. Schultz W. Multiple dopamine functions at different time courses. Annu Rev Neurosci 2007;30(1):259–88
20. Young AMJ, Ahier RG, Upton RL, et al. Increased extracellular dopamine in the nucleus accumbens of the rat during associative learning of neutral stimuli. Neuroscience 1998;83(4):1175–83
21. Violin JD, DiPilato LM, Yildirim N, et al. beta2-adrenergic receptor signaling and desensitization elucidated by quantitative modeling of real time cAMP dynamics. J Biol Chem 2008;283(5):2949–61
22. Ingalls BP. Mathematical Modeling in Systems Biology: an introduction [Internet]. MIT Press; 2013. 1-396 p
23. Ögren SO, Hall H, Köhler C, et al. Remoxipride, a new potential antipsychotic compound with selective anti-dopaminergic actions in the rat brain. Eur J Pharmacol 1984;102:459–74
24. Hall DA, Strange PG. Evidence that antipsychotic drugs are inverse agonists at D2 dopamine receptors. Br J Pharmacol 1997;121(4):731–6
25. Bond RA, IJzerman AP. Recent developments in constitutive receptor activity and inverse agonism, and their potential for GPCR drug discovery. Trends Pharmacol Sci 2006;27(2):92–6
26. Ang J, Ingalls B, McMillen D. Probing the inputoutput behavior of biochemical and genetic systems: System identification methods from control theory [Internet]. 1st ed. Methods in Enzymology. Elsevier Inc.; 2011. 279-317 p
27. Schiele F, Ayaz P, Fernández-Montalván A. A universal, homogenous assay for high throughput determination of binding kinetics. Anal Biochem 2014;468:42–9
28. Nederpelt I, Georgi V, Schiele F, et al. Characterization of 12 GnRH peptide agonists - A kinetic perspective. Br J Pharmacol 2016;173(1):128–41
29. Cheng Y-C, Prusoff WH. Relationship between the inhibition constant (KI) and the concentration of inhibitor which causes 50 per cent inhibition (I50) of an enzymatic reaction. Biochem Pharmacol 1973;22(23):3099–108

30. Motulsky HJ, Mahan LC. The Kinetics of Competitive Radioligand Binding Predicted Mass Action by the Law of Mass Action. Mol Pharmacol 1984;25(1):1–9
31. Fang, Frutos, Verklereen. Label-free cell-based assays for GPCR screening. Comb Chem High Throughput Screen 2008;11(5):357–69
32. de Ligt RAF, Kourounakis AP, IJzerman AP. Inverse agonism at G protein-coupled receptors: (patho)physiological relevance and implications for drug discovery. Br J Pharmacol 2000;130(1):1–12
33. Cherry JA, Pho V. Characterization of cAMP Degradation by Phosphodiesterases in the Accessory Olfactory System. Chem Senses 2002;27(7):643–52
34. Keravis T, Lugnier C. Cyclic nucleotide phosphodiesterase (PDE) isozymes as targets of the intracellular signalling network: benefits of PDE inhibitors in various diseases and perspectives for future therapeutic developments. Br J Pharmacol 2012;165:1288–305
35. R Core Team. R: A language and environment for statistical computing. R Found Stat Comput Vienna, Austria URL http//wwwR-project.org/ 2013;
36. Soetaert K, Petzoldt T, Setzer RW. Solving Differential Equations in R: Package deSolve. J Stat Softw 2010;33(9):1–25
37. Burstein ES, Ma J, Wong S, et al. Intrinsic Efficacy of Antipsychotics at Human D 2 , D 3 , and D 4 Dopamine Receptors : Identification of the Clozapine Metabolite N -Desmethylclozapine as a D 2 / D 3 Partial Agonist. J Pharmacol Exp Ther 2005;315(3):1278–87
38. Wood M, Dubois V, Scheller D, et al. Rotigotine is a potent agonist at dopamine D_1 receptors as well as at dopamine D_2 and D_3 receptors. Br J Pharmacol 2015;172(4):1124–35
39. Kroeze WK, Hufeisen SJ, Popadak BA, et al. H1-Histamine Receptor Affinity Predicts Short-Term Weight Gain for Typical and Atypical Antipsychotic Drugs. Neuropsychopharmacology 2003;28(3):519–26
40. Toll L, Berzetei-Gurske IP, Polgar WE, et al. Standard binding and functional assays related to medications development division testing for potential cocaine and opiate narcotic treatment medications. NIDA Res Monogr 1998;178:440–66
41. Seeman P, Tallerico T. Antipsychotic drugs which elicit little or no parkinsonism bind more loosely than dopamine to brain D2 receptors, yet occupy high levels of these receptors. Mol Psychiatry 1998;3(2):123–34
42. Richelson E, Souder T. Binding of antipsychotic drugs to human brain receptors focus on newer generation compounds. Life Sci 2000;68(1):29–39
43. Leysen JE, Gommeren W. Drug-Receptor Dissociation Time , New Tool for Drug Research : Receptor Binding Affinity and Drug-Receptor Dissociation Profiles of Serotonin-S2 , Dopamine-D2 , Histamine-HI Antagonists , and Opiates. Drug Dev Res 1986;131:119–31
44. Kongsamut S, Kang J, Chen XL, et al. A comparison of the receptor binding and HERG channel affinities for a series of antipsychotic drugs. Eur J Pharmacol 2002;450(1):37–41
45. Klein Herenbrink C, Sykes DA, Donthamsetti P, et al. The role of kinetic context in apparent biased agonism at GPCRs. Nat Commun 2016;7:10842
46. Freedman SB, Patel S, Marwood R, et al. Expression and pharmacological characterization of the human D3 dopamine receptor. J Pharmacol Exp Ther 1994;268(1):417–26
47. Sahlholm K, Zeberg H, Nilsson J, et al. The fast-off hypothesis revisited: A functional kinetic study of antipsychotic antagonism of the dopamine D2 receptor. Eur Neuropsychopharmacol 2016;26(3):467–76
48. Schröder R, Janssen N, Schmidt J, et al. Deconvolution of complex G protein–coupled receptor signaling in live cells using dynamic mass redistribution measurements. Nat Biotechnol 2010;28(9):943–9
49. Zou L-L, Cai S-T, Jin G-Z. Chronic treatment with (-)-stepholidine alters density and turnover of D1 and D2 receptors in striatum. Acta Pharmacol Sin 1996;17(6):485–9
50. Dewar KM, Paquet M, Reader TA. Alterations in the turnover rate of dopamine D1 but not D2 receptors in the adult rat neostriatum after a neonatal dopamine denervation. Neurochem Int 1997;30(6):613–21

Supplemental information

Supplement S 1. Measurements of binding kinetics and equilibrium binding for antagonists and agonist at room temperature and at 37 °C.

Table S 1. Binding equilibrium (ePCA) and binding kinetics (kPCA) measurements at 37°C. NA: not available, NPA: N-n-Propyl Apomorphine

	ePCA				kPCA			
Compound ID	**K_I [M]**	**SD**	**K_D [M]**	**SD**	**k_{on} [1/(M*s)]**	**SD**	**k_{off} [1/s]**	**SD**
(-)-Nemonapride	2.11E-10	5.96E-11	4.96E-11	3.54E-11	1.79E+07	1.95E+06	8.54E-04	5.38E-04
(-)-Quinpirole	> 8.71E-07	NA	3.83E-06	2.84E-06	5.35E+04	2.42E+04	1.45E-01	1.47E-01
Aripiprazole	1.03E-09	4.29E-10	5.58E-10	4.90E-11	1.77E+06	6.03E+05	1.00E-03	4.23E-04
Bromocriptine	1.75E-09	4.04E-10	5.86E-10	3.22E-12	2.40E+05	8.64E+04	1.41E-04	5.14E-05
Bromperidol	3.24E-09	1.55E-09	2.52E-09	8.27E-10	2.67E+06	1.04E+06	7.42E-03	2.68E-03
Cabergoline	8.22E-10	1.03E-10	7.38E-10	6.89E-11	2.11E+06	4.75E+05	1.54E-03	2.06E-04
Clozapine	3.12E-08	1.96E-09	5.39E-08	1.33E-08	8.35E+05		2.88E-02	
Domperidone	5.06E-09	8.69E-10	3.15E-09	3.92E-10	6.87E+05	2.62E+05	2.12E-03	5.56E-04
Dopamine	> 8.71E-07		1.07E-06	4.99E-07	1.02E+04	6.02E+03	9.36E-03	1.32E-03
JNJ-37822681	1.61E-08	1.89E-09	1.93E-08	3.99E-09	1.24E+06	9.63E+05	2.19E-02	1.36E-02
JNJ-39269646	7.22E-08	1.18E-08	9.14E-08	1.37E-08	1.71E+05	NA	1.84E-02	NA
Haloperidol	9.48E-10	2.96E-10	3.86E-10	9.95E-11	7.23E+07	NA	3.30E-02	NA
Memantine	> 8.71E-07	NA	1.01E-05	2.59E-07	1.99E+03	1.37E+03	2.41E-02	9.94E-03
NPA	3.40E-08	8.42E-09	1.77E-07	6.90E-08	NA	NA	NA	NA
Olanzapine	1.39E-08	1.29E-09	2.17E-08	9.44E-09	1.61E+06	1.00E+06	3.61E-02	5.99E-03
Paliperidone	8.18E-09	1.56E-09	9.25E-09	2.71E-09	1.92E+06	1.56E+06	1.36E-02	5.91E-03
Pergolide	1.30E-08	6.53E-09	2.87E-08	1.11E-08	3.27E+06	NA	7.89E-02	NA
Pimozide	6.62E-10	3.27E-10	5.82E-10	1.40E-10	9.38E+05	5.11E+05	5.10E-04	1.66E-04
Piribedil	2.99E-07	4.02E-08	4.22E-07	5.13E-08	2.23E+04	NA	8.25E-03	NA
Quetiapine	1.63E-07	3.84E-09	1.60E-07	9.72E-08	6.74E+05	4.03E+05	1.03E-01	5.98E-02
R-(-)-Apomorphine	1.69E-07	7.42E-09	2.71E-07	2.11E-07	> 5.92E+04	NA	> 1.00E-02	NA
Remoxipride	1.23E-07	2.81E-08	1.35E-07	2.86E-08	1.10E+06	4.54E+05	1.30E-01	7.94E-02
Risperidone	1.67E-09	9.11E-10	1.30E-09	7.52E-10	8.41E+06	5.96E+06	1.07E-02	5.02E-03
Rotigotine	1.67E-08	4.25E-09	5.69E-09	1.68E-09	3.18E+06	8.05E+05	1.74E-02	7.63E-04
S-(+)-Apomorphine	5.16E-07	6.50E-08	5.47E-07	1.75E-07	2.13E+04	NA	9.94E-03	NA
Sertindole	6.80E-09	1.86E-09	7.52E-09	5.87E-10	1.33E+06	NA	9.45E-03	NA
Spiperone	5.09E-10	2.29E-10	6.58E-11	1.77E-11	2.03E+07	7.02E+06	1.45E-03	6.22E-04
S-(+)-Raclopride	2.19E-09	1.85E-09	1.29E-09	1.18E-10	2.43E+06	8.68E+05	3.08E-03	8.32E-04
Ziprasidone	1.65E-09	2.93E-10	2.28E-09	2.12E-10	3.54E+06	1.38E+06	7.92E-03	2.31E-03

Table S 2. Binding equilibrium (ePCA) and binding kinetics (kPCA) measurements at room temperature. NA: not available, NPA: N-n-Propyl Apomorphine

	ePCA				kPCA			
Compound ID	**K_i [M]**	**SD**	**K_D [M]**	**SD**	**k_{on} [1/(M*s)]**	**SD**	**k_{off} [1/s]**	**SD**
(-)-Nemonapride	2.70E-10	5.96E-12	9.58E-11	3.26E-12	5.66E+06	2.73E+05	5.43E-04	4.46E-05
(-)-Quinpirole	> 8.53E-07	NA	7.80E-07	6.28E-07	1.07E+05	4.77E+04	9.82E-02	1.04E-01
Aripiprazole	1.01E-09	3.46E-10	2.39E-10	4.40E-13	7.24E+05	3.17E+05	1.73E-04	7.52E-05
Bromocriptine	5.04E-09	1.98E-09	2.19E-10	1.96E-10	8.09E+04	2.54E+04	2.02E-05	1.80E-05
Bromperidol	3.09E-09	3.22E-10	1.89E-09	7.49E-10	2.26E+06	9.57E+05	3.91E-03	1.21E-04
Cabergoline	9.58E-10	2.89E-10	4.26E-10	2.13E-10	8.80E+05	5.13E+05	3.21E-04	3.15E-05
Clozapine	3.42E-08	3.93E-09	5.05E-08	1.28E-08	1.20E+06	1.44E+06	5.13E-02	5.74E-02
Domperidone	4.18E-09	1.08E-09	3.04E-09	5.08E-10	1.81E+05	5.26E+04	5.37E-04	6.75E-05
Dopamine	> 8.53E-07		1.27E-06	5.56E-07	1.88E+04	2.16E+04	2.82E-02	3.01E-02
JNJ-37822681	1.24E-08	2.14E-09	9.32E-09	2.71E-09	7.33E+05	NA	9.54E-03	NA
JNJ-39269646	3.96E-08	2.10E-09	4.87E-08	8.35E-09	4.53E+06	4.51E+06	1.79E-01	1.64E-01
Haloperidol	9.88E-10	1.55E-10	3.82E-10	4.98E-11	1.21E+07	5.18E+06	4.48E-03	1.37E-03
Memantine	> 8.53E-07	NA	2.61E-05	9.91E-06	2.98E+02	NA	1.07E-02	NA
NPA	2.42E-08	3.80E-09	NA	NA	NA	NA	NA	NA
Olanzapine	1.37E-08	9.41E-10	8.58E-09	3.38E-09	> 7.30E+05	NA	> 1.00E-02	NA
Paliperidone	7.39E-09	9.15E-10	5.45E-09	2.07E-09	6.81E+05	1.83E+05	3.52E-03	4.14E-04
Pergolide	1.33E-08	6.02E-09	2.44E-08	1.24E-08	9.81E+05	NA	2.59E-02	NA
Pimozide	1.22E-09	4.23E-10	2.55E-10	6.74E-11	3.10E+05	2.45E+05	7.08E-05	4.17E-05
Piribedil	2.26E-07	2.77E-08	2.23E-07	5.90E-08	4.43E+04	9.30E+03	1.21E-02	4.18E-03
Quetiapine	1.26E-07	3.48E-08	1.50E-07	6.94E-08	1.03E+05	2.04E+04	1.69E-02	6.07E-03
R-(-)-Apomorphine	1.13E-07	1.88E-08	1.70E-07	7.68E-08	> 8.85E+04	NA	> 1.00E-02	NA
Remoxipride	7.01E-08	1.08E-08	8.31E-08	3.47E-08	3.28E+05	NA	3.14E-02	NA
Risperidone	1.05E-09	4.07E-10	7.56E-10	7.62E-11	4.43E+06	8.54E+05	3.31E-03	3.09E-04
Rotigotine	1.16E-08	3.55E-11	7.82E-09	2.86E-09	3.84E+06	3.78E+06	2.65E-02	2.75E-02
S-(+)-Apomorphine	2.65E-07	8.49E-08	3.33E-07	1.15E-07	2.94E+04	NA	1.36E-02	NA
Sertindole	6.15E-09	3.21E-09	4.07E-09	2.23E-09	7.70E+05	7.00E+05	2.35E-03	1.13E-03
Spiperone	2.96E-10	1.43E-10	1.79E-10	4.11E-12	5.44E+06	1.11E+06	9.70E-04	1.76E-04
S-(+)-Raclopride	1.35E-09	9.97E-10	6.34E-10	1.15E-10	9.57E+05	1.81E+05	5.96E-04	4.62E-06
Ziprasidone	1.76E-09	4.12E-10	1.31E-09	8.40E-11	1.29E+06	2.01E+05	1.67E-03	1.55E-04

Figure S1a

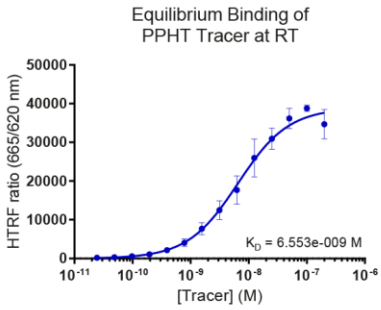

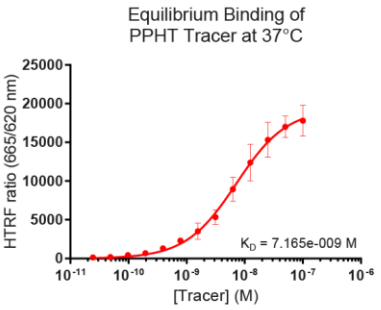

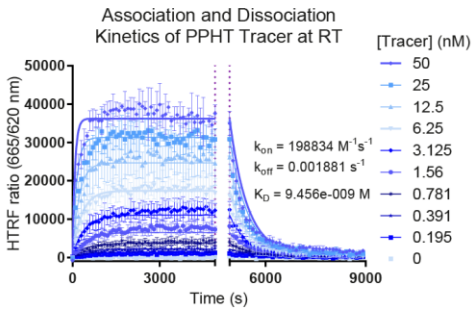

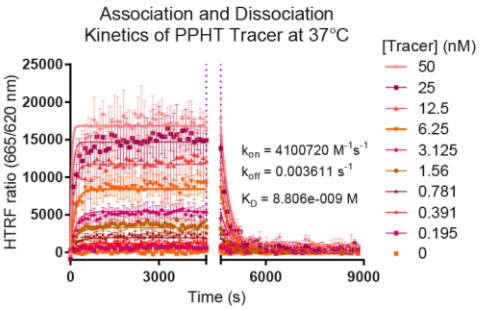

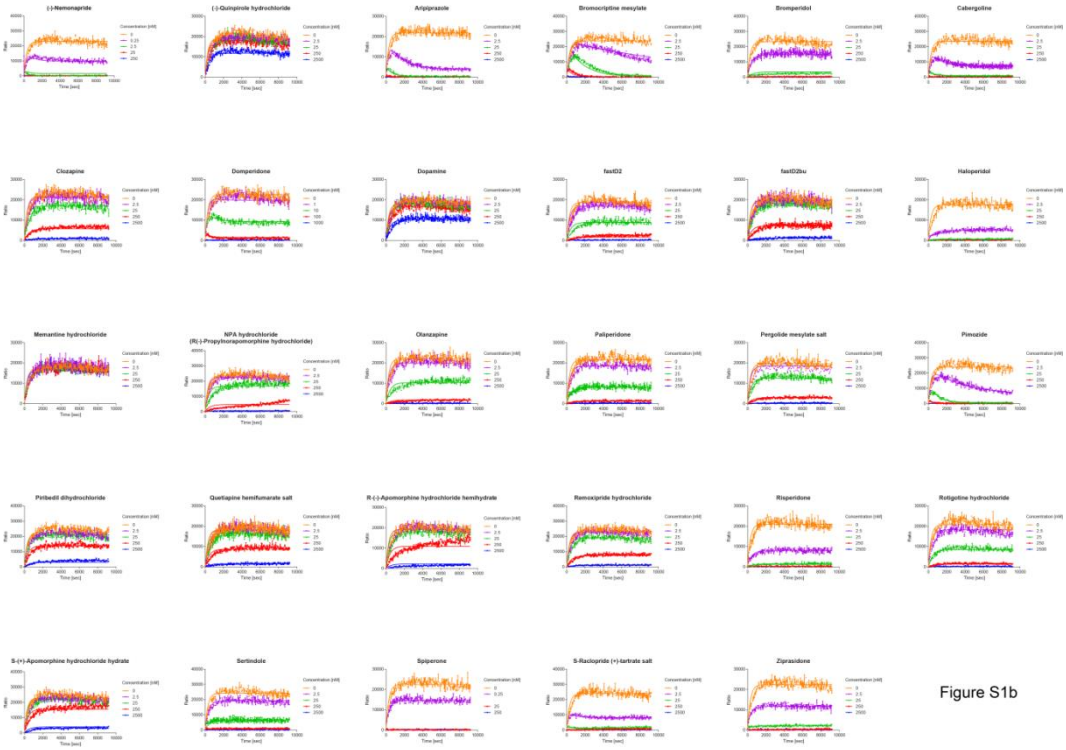

Figure S1b

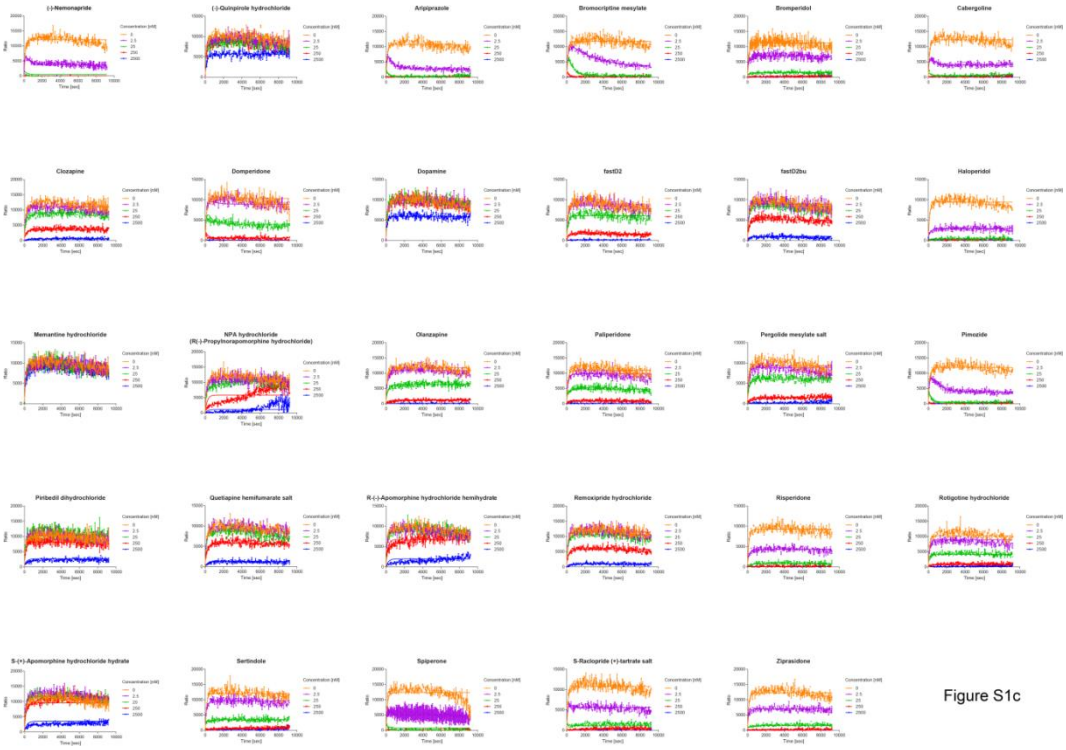

Figure S1c

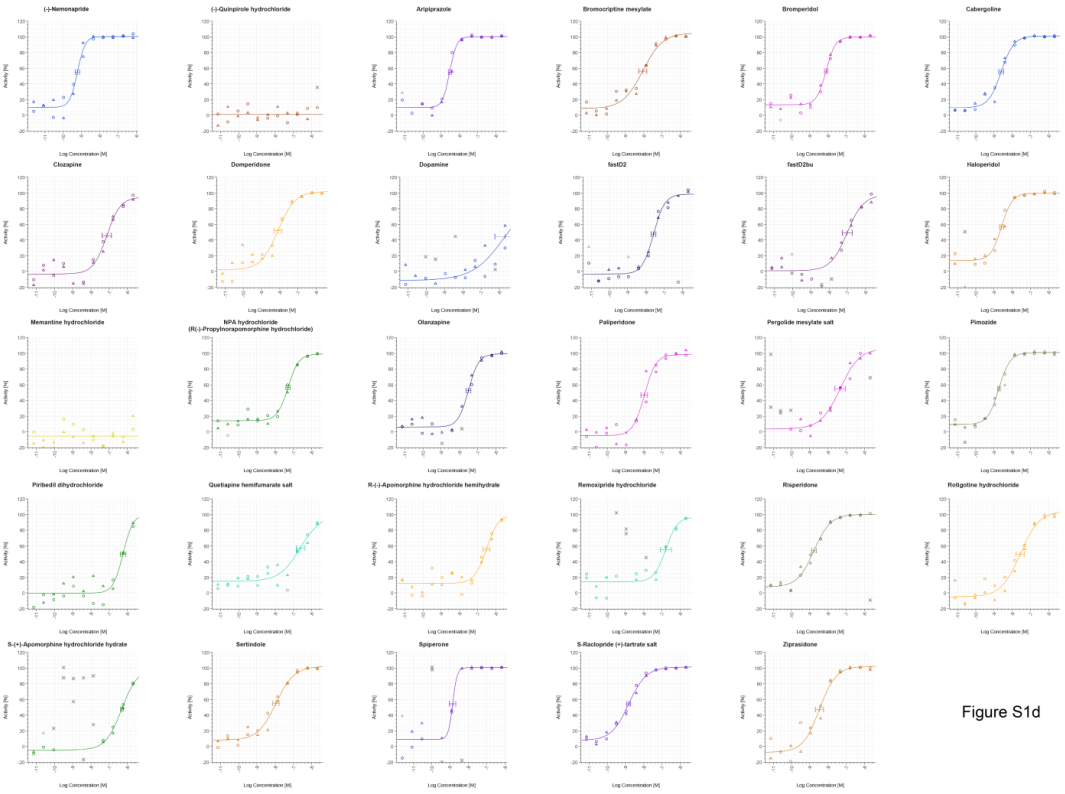

Figure S1d

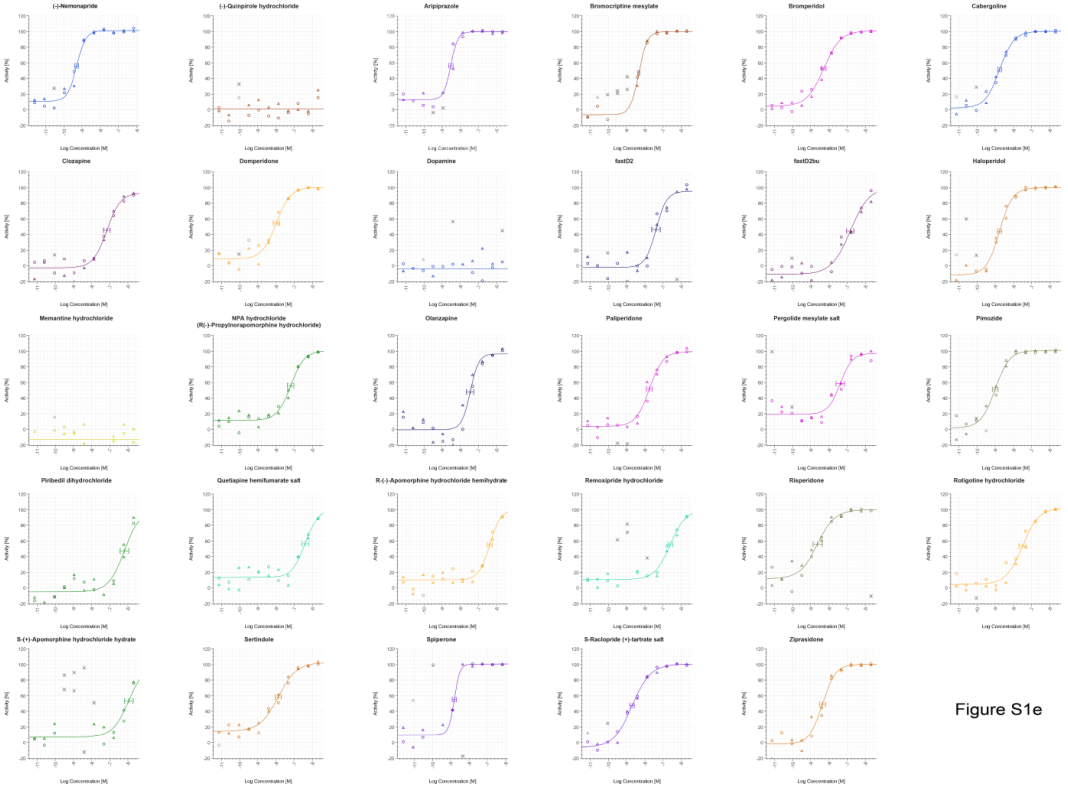

Figure S 1. Determination of affinity and kinetic parameters for the binding of Dopamine D2 receptor drugs using the TagLite® homogeneous time resolved fluorescence (HTRF) technology and the equilibrium and kinetic Probe Competition Assays (ePCA and kPCA). Symbols represent the measured data and lines the fits to the corresponding binding models. The compounds indicated with fastD2 and fastD2bu refer to JNJ-37822681 and JNJ-39269646, respectively. These figures are also available as separate supplemental files to allow better readability.

a) Characterization of the PPHT tracer used in ePCA and kPCA at room temperature and at 37°C. The upper panel shows representative steady state titration curves, and the lower panel kinetic association- and dissociation curves at increasing tracer concentrations. HTRF signals were fit to the models specified in the methods section and the resulting binding parameters are indicated in the graphs.

b-c) Representative kPCA traces of the compounds listed in Table S1 at room temperature (b) and 37°C (c). Compound names are indicated on top of the graphs and dosing on the right-hand side.

d-e) Representative ePCA curves of the compounds listed in Table S1 at room temperature (d) and 37°C (e). Compound names are indicated on top of the graphs and dosing on the right-hand side. Grey crosses indicate data points excluded from the analysis. The different symbols represent different dilution series.

Supplement S 2. DMR experimental overview and results for all D_2 antagonists.

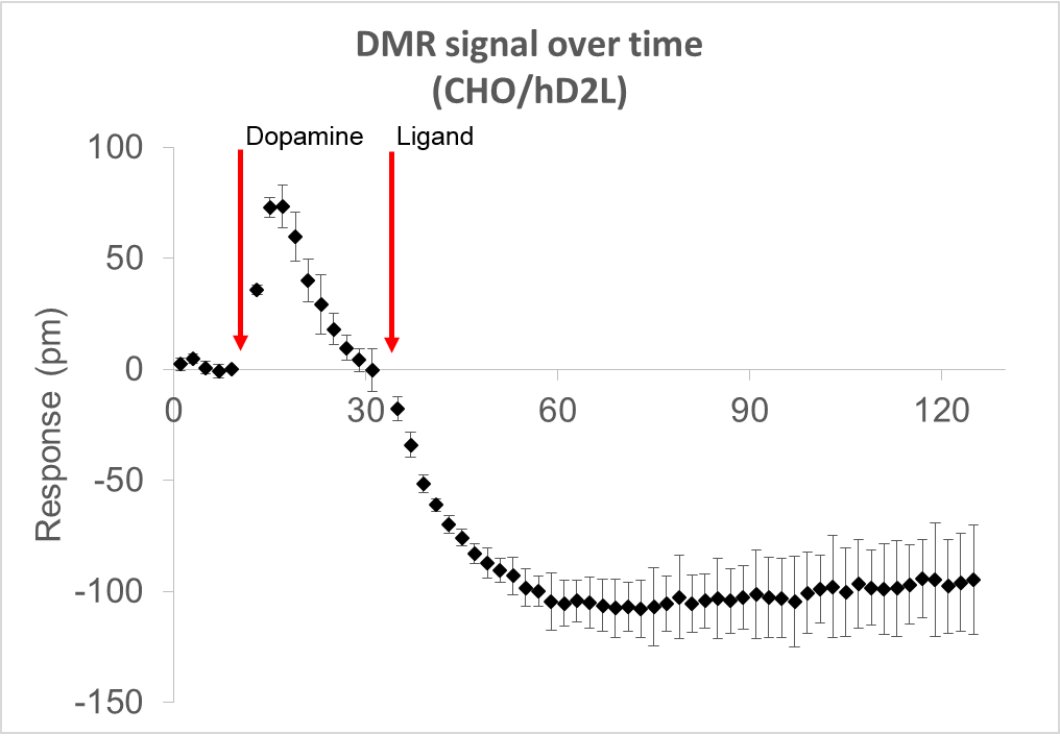

Figure S 2 Example of the complete DMR versus time curve for 10 µM haloperidol. The time points of addition of dopamine and the ligand (haloperidol in this case) are indicated with the red arrows.

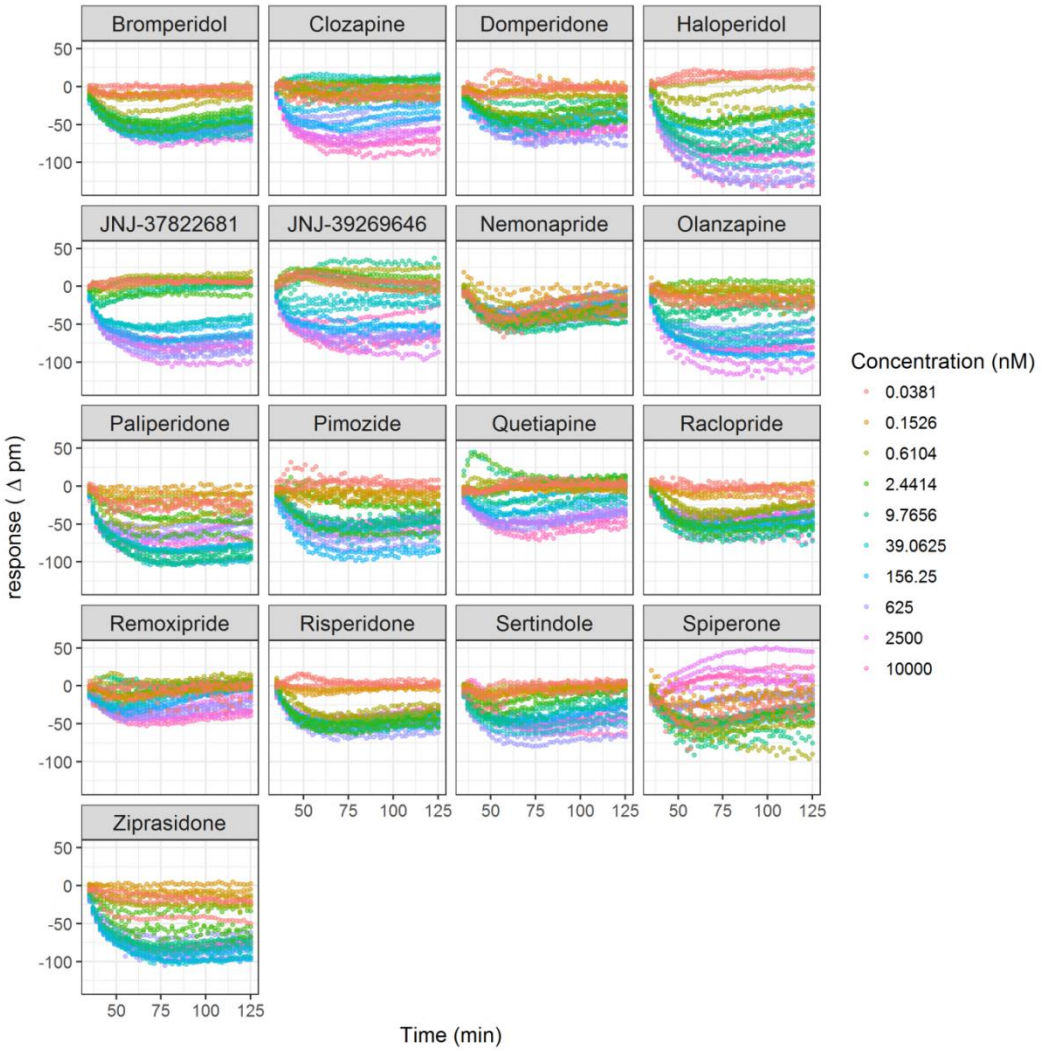

Figure S 3. Normalized Dynamic Mass Redistribution (DMR) responses as change in DMR response in picometer compared to the dopamine response after addition of various concentrations of the indicated antagonists. Normalization was performed by subtracting the response per well/replicate at the latest time point after dopamine addition and before antagonist addition (t = 31 min) from the raw DMR traces. Normalization for the dopamine + buffer was performed for each time point by subtracting the mean dopamine + buffer in each experiment/well plate from the normalized DMR traces.

Supplement S 3. Model 1 equations and parameter estimates for all dopamine D_2 antagonists.

To describe dopamine and antagonist binding to the D_2 receptor, a simple drug-target binding model with competition between antagonist and dopamine was developed. This model assumed a constant total receptor concentration. This was represented as a single conservation equation of total receptor (R_t), where the receptor can have 3 different states: free receptor (R), antagonist bound to receptor (RL) and dopamine bound to receptor (RDA). Receptor recycling (RR) was added to this model as well, which describes internalization of the receptor-agonist complex, dissociation of this complex return of the free receptor to the cell membrane. This model is given by the following equations (equation 1-5):

$$\frac{d[L]}{dt} = -k_{onL}[R][L] + k_{offL}[RL]$$

(Eq. 1)

$$\frac{d[DA]}{dt} = -k_{onDA}[R][DA] + k_{offDA}[RDA] + RR[RDA]$$

(Eq. 2)

$$\frac{\mathrm{d[RL]}}{\mathrm{dt}} = k_{onL}[R][L] - k_{offL}[RL]$$

(Eq. 3)

$$\frac{\mathrm{d[RDA]}}{\mathrm{dt}} = k_{onDA}[R][DA] - k_{offDA}[RDA] - RR[RDA]$$

(Eq. 4)

$$[R] = [R_t] - [RL] - [RDA]$$

(Eq. 5)

In these equations, [L] represents the free antagonist concentration, [DA] represents the free dopamine concentration, [R_t] represents the total receptor concentration, [R] represents the free receptor concentration, [RL] represents the concentration of the receptor—antagonist complex and [RDA] represents the concentration of the receptor—dopamine complex. k_{onL} and k_{onDA} represent the second-order association rate constants of receptor with the antagonist and with dopamine, respectively. k_{offL} and k_{offDA} represent the first order dissociation rate constants of the antagonist and dopamine from the receptor-bound complex, respectively. The receptor binding part of the model as described above was connected to cAMP concentrations in a mechanistic manner according to the following equations (equation 6 and 7).

$$\frac{d[cAMP]}{dt} = \left(k_1 + \frac{k_{0,max}[RL]^n}{EC50^n + [RL]^n}\right)\left(1 - \frac{[RDA]^n}{IC50^n + [RDA]^n}\right) - k_2[cAMP] - k_3[cAMP][PDE]$$

(Eq. 6)

Here, $k_{0,max}$ represents the maximum rate constant for inverse agonism by the receptor-antagonist complex, where n is the hill coefficient. Additionally, k_1 represents the rate constant for baseline synthesis of cAMP by adenylyl cyclase. Furthermore, the total cAMP synthesis is inhibited by the receptor dopamine complex (RDA) in a nonlinear manner, where n is the hill coefficient as well. k_2 is the rate constant for cAMP elimination independent of active PDE, and k_3 is the rate constant of active PDE-mediated cAMP elimination. active PDE synthesis is dependent on the cAMP concentration, and active PDE degradation is determined by the first order rate constant k_5 as in equation 7.

$$\frac{d[PDE]}{dt} = k_4[cAMP] - k_5[PDE]$$

(Eq. 7)

Table S 3. Parameter estimates from fitting the final model to the cAMP response data. Asterisks indicate parameter values that were not estimated but used as input parameter values. $DAFR_{50}$ denotes the ratio of the total receptor concentration divided by the dopamine-bound bound receptor concentration that inhibits the cAMP synthesis to 50%, LFR_{50} denotes the ratio of the total receptor concentration divided by the antagonist bound receptor concentration that generates the half-maximal antagonist-dependent cAMP synthesis (i.e. k_0 equals 0.5 * k_{0max}), R_{tot} denotes the total receptor concentration, k_{0max} denotes the maximal value of k_0.

Parameter (unit)	Value	RSE
k_{off} Bromperidol (min^{-1})	0.235*	
k_{off} Clozapine (min^{-1})	3.08*	
k_{off} Domperidone (min^{-1})	0.0322*	
k_{off} JNJ-39269646 (min^{-1})	10.7*	
k_{off} JNJ-37822681 (min^{-1})	0.573*	
k_{off} Haloperidol (min^{-1})	0.269*	
k_{off} Nemonapride (min^{-1})	0.0326*	
k_{off} Olazapine (min^{-1})	0.600*	
k_{off} Paliperidone (min^{-1})	0.211*	
k_{off} Pimozide (min^{-1})	0.0042*	
k_{off} Quetiapine (min^{-1})	1.01*	
k_{off} Raclopride (min^{-1})	0.0358*	
k_{off} Remoxipride (min^{-1})	1.89*	
k_{off} Risperidone (min^{-1})	0.199*	
k_{off} Sertindole (min^{-1})	0.141*	
k_{off} Spiperone (min^{-1})	0.0582*	
k_{off} Ziprasidone (min^{-1})	0.1*	
K_D Bromperidol (nM)	2.04	2.0%
K_D Clozapine (nM)	440	2.1%
K_D Domperidone (nM)	1.72	2.1%
K_D JNJ-39269646 (nM)	104	1.9%
K_D JNJ-37822681 (nM)	19.5	1.9%
K_D Haloperidol (nM)	1.72	2.4%
K_D Nemonapride (nM)	0.454	2.2%
K_D Olazapine (nM)	22.7	2.3%
K_D Paliperidone (nM)	1.61	2.4%
K_D Pimozide (nM)	291	2.8%
K_D Quetiapine (nM)	942	2.2%
K_D Raclopride (nM)	8.29	2.2%
K_D Remoxipride (nM)	118	2.7%
K_D Risperidone (nM)	10.5	4.6%

K_D Sertindole (nM)	6.89	2.0%
K_D Spiperone (nM)	0.19	2.5%
K_D Ziprasidone (nM)	3.56	1.8%
K_D Dopamine (nM)	10.3	3.9%
k_{off} Dopamine (min^{-1})	1.69*	
R_{tot} [D2 Receptor concentration] (nM)	1.74	1.3%
k_{0max}: Maximum cAMP synthesis induced by inverse agonism (min^{-1})	20.5	0.5%
k_1: Baseline cAMP synthesis (min^{-1})	4.12	0.8%
k_2: cAMP degradation independent from active PDE (min^{-1})	0.0334	10.8%
k_3: cAMP degradation by active PDE (nM^{-1} min^{-1})	0.00882	0.2%
k_4: active PDE synthesis (min^{-1})	0.00882[a]	
k_5: active PDE degradation (min^{-1})	0.0005*	
$DAFR_{50}$ Dopamine	2.25	2.4%
Hill coefficient	1.77	0.4%
LFR_{50} Bromperidol	1.54	0.6%
LFR_{50} Clozapine	0.504	0.7%
LFR_{50} Domperidone	1.71	0.6%
LFR_{50} JNJ-39269646	0.856	0.5%
LFR_{50} JNJ-37822681	0.823	0.4%
LFR_{50} Haloperidol	0.699	0.5%
LFR_{50} Nemonapride	2.47	1.1%
LFR_{50} Olazapine	0.628	0.6%
LFR_{50} Paliperidone	0.657	0.5%
LFR_{50} Pimozide	618	1.9%
LFR_{50} Quetiapine	0.827	0.9%
LFR_{50} Raclopride	2.68	1.2%
LFR_{50} Remoxipride	1.95	1.4%
LFR_{50} Risperidone	5.37	3.6%
LFR_{50} Sertindole	1.02	0.5%
LFR_{50} Spiperone	1.56	0.6%
LFR_{50} Ziprasidone	0.959	0.4%
Receptor Turnover (min^{-1})	0.238	2.2%
Proportional error	0.01	0.3%

[a] k_4 was set to have the same value as k_3.

Supplement S 4. explanation of frequency response analysis results (FRA)

In a frequency response analysis, the dynamic behavior of a system is investigated by providing a harmonic oscillation as input signal, described by a sine wave with a variable frequency. Subsequently, the amplitude and the phase of the resulting sine wave are compared to that of the original sine wave. This frequency response analysis is often applied to a linear or linearized system and is derived analytically from the system's differential equations, but can also be derived from experimental data or simulations [26]. Dopamine concentrations are released in a pulsatile manner with a frequency of around 1 s^{-1}, but also show more slowly fluctuating levels caused by transient activity. Therefore, a frequency response analysis with fluctuating dopamine concentrations as input is reflective of the relevant context of drug action for dopamine antagonists.

Here we show the intermediate steps that lead to the eventual calculation of gain in cAMP amplitude. Firstly, we show in the top row of Figure S 4 three examples of different input frequencies, for which the different line colors all have the same overlaying sine wave characteristics and are not influenced by the drug-target k_{off}.

The second row of Figure S 4 shows how the dopamine occupancy follows the dopamine concentrations (in a non-linear fashion) until the frequency gets too high, as visible for the highest frequency, and the amplitude of the dopamine occupancy fluctuation declines. The slight influence of the antagonist k_{off} on dopamine occupancy for the intermediate occupancy can be explained by the competitive binding of the antagonist and dopamine and the influence of the koff on antagonist binding, as shown in the third row of Figure S 4.

The third row of Figure S 4 shows how all antagonists can be displaced by dopamine binding for the slowest frequency (hence the fluctuating occupancy), while for the intermediate frequency only the fast dissociating drug can be displaced fast enough to keep the original amplitude. Finally, for the highest frequency, none of the antagonists can be displaced fast enough and the fluctuation in dopamine concentrations and dopamine occupancy is not reflected in the antagonist-receptor occupancy.

The bottom row of Figure S 4 shows how the differences in dopamine and antagonist occupancy are translated into cAMP concentrations in a frequency-dependent manner (note the increased gain for the intermediate frequency that is not reflected in the occupancy profiles).

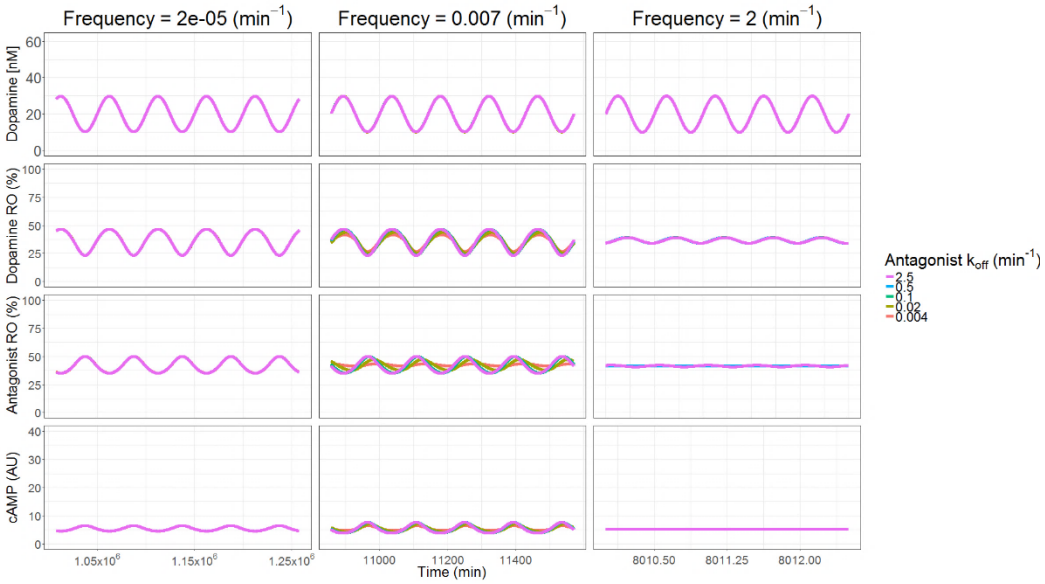

Figure S 4. Example of input frequencies for dopamine as used in the simulations (top panels) and the simulated responses (lower panels). The second row shows the dopamine receptor occupancy, the third row the antagonist receptor occupancy and the bottom row the cAMP response for each simulation with the fluctuating dopamine concentrations from the corresponding top row panels. The different line colors represent different simulations for which the dissociation rate constant of the antagonist-receptor complex is changed. The dopamine fluctuation frequencies are indicated above the panels and by the different time scales on the x-axis.

Supplement S 5. Identification of the influence of system-specific parameters on the frequency response analysis results.

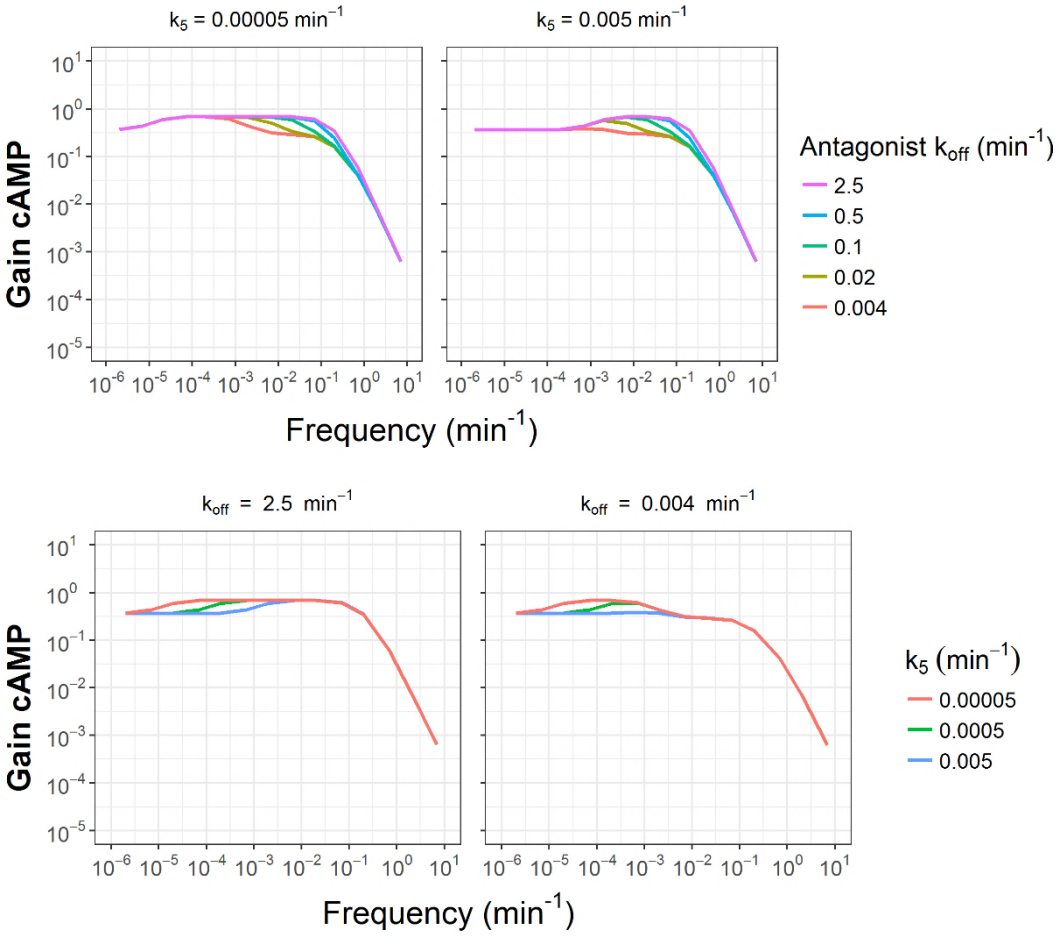

Figure S 5. Frequency response analysis for 3 different active PDE turnover rate constants and 5 different antagonist k_{off} values. The upper plots show the influence of k_{off} for two different active PDE turnover rate constants, and the lower plots show the influence of the active PDE turnover rate constants for two different koff values. The input signal was a sine wave of free dopamine with an amplitude of 10nM and baseline of 20 nM, at the frequencies indicated on the x-axis. At each active PDE turnover rate, 5 different antagonist k_{off} values were simulated, which are represented by the different line colors. The k_{on} values were changed simultaneously with k_{off}, which means that the K_D was constant at 6.93 nM. The antagonist concentration was 14 nM, the LFR_{50} was 1.03 and all system-specific parameters were identical to Table 3. The order of the lines in the legend follows the order of the lines in the graph.

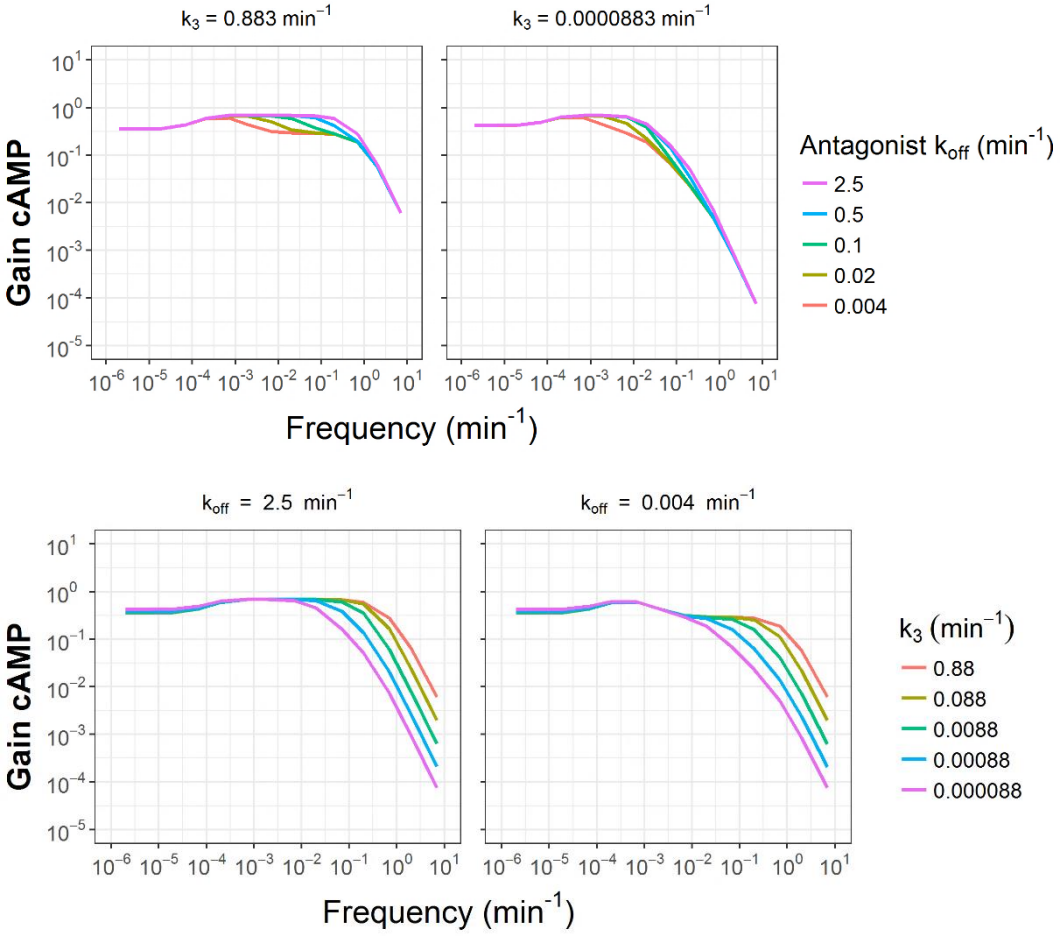

*Figure S 6. Frequency response analysis for active PDE-dependent cAMP turnover rate constants (k_3) of 0.883 min^{-1} (left) and 0.883*10^{-4} min^{-1} (right). The input signal was a sine wave of free dopamine with an amplitude of 10nM and baseline of 20 nM, at the frequencies indicated on the x-axis. At each cAMP turnover rate, 5 different antagonist k_{off} values were simulated, which are represented by the different line colors. The k_{on} values were changed simultaneously with k_{off}, which means that the K_D was constant at 6.93 nM. The antagonist concentration was 14 nM, the LFR_{50} was 1.03 and all system-specific parameters were identical to* Table 3*. The order of the lines in the legend follows the order of the lines in the graph.*

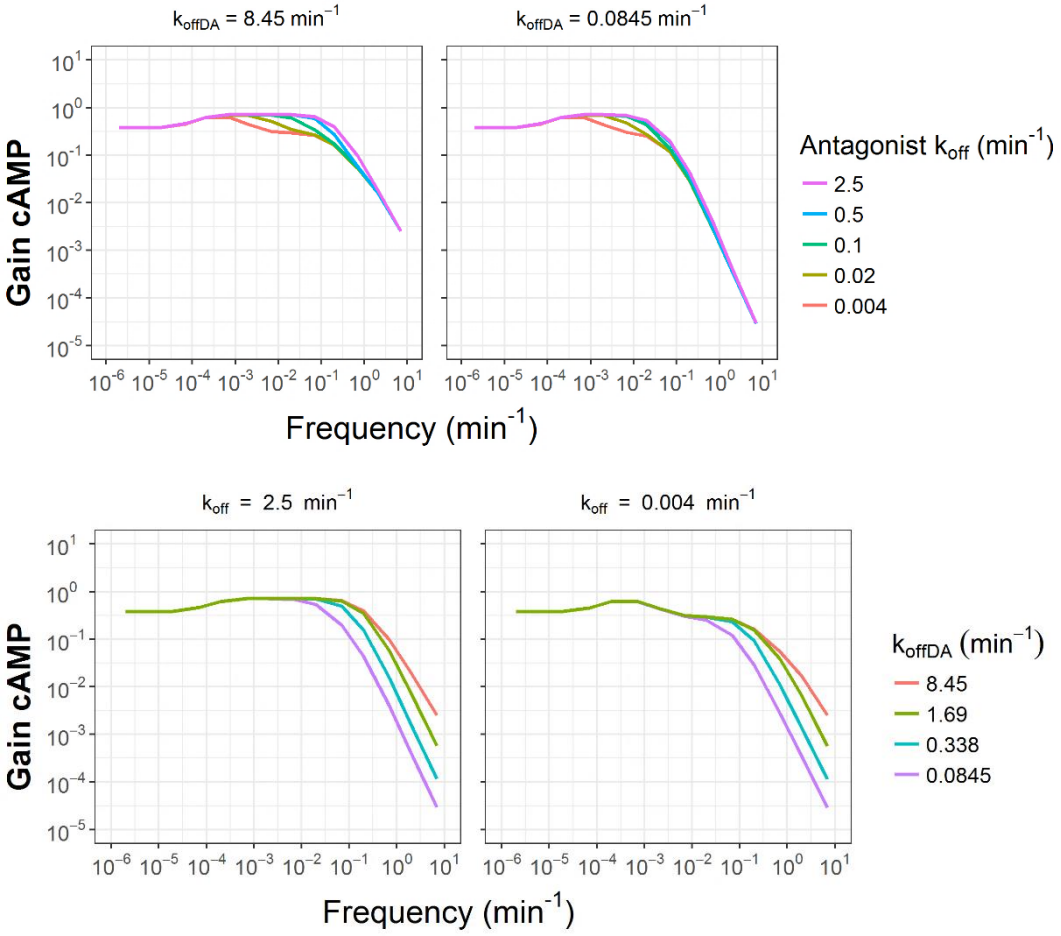

Figure S 7. Frequency response analysis for dopamine-receptor dissociation rate constants (k_{offDA}) of 8.45 min^{-1} (left) and 0.0845 min^{-1} (right). The input signal was a sine wave of free dopamine with an amplitude of 10nM and baseline of 20 nM, at the frequencies indicated on the x-axis. At each dopamine dissociation rate constant, 5 different antagonist k_{off} values were simulated, which are represented by the different line colors. The k_{on} values were changed simultaneously with k_{off}, which means that the K_D was constant at 6.93 nM. The antagonist concentration was 14 nM, the LFR_{50} was 1.03 the receptor recycling rate constant was switched to 0 and all other system-specific parameters were identical to Table 3*. The order of the lines in the legend follows the order of the lines in the graph.*

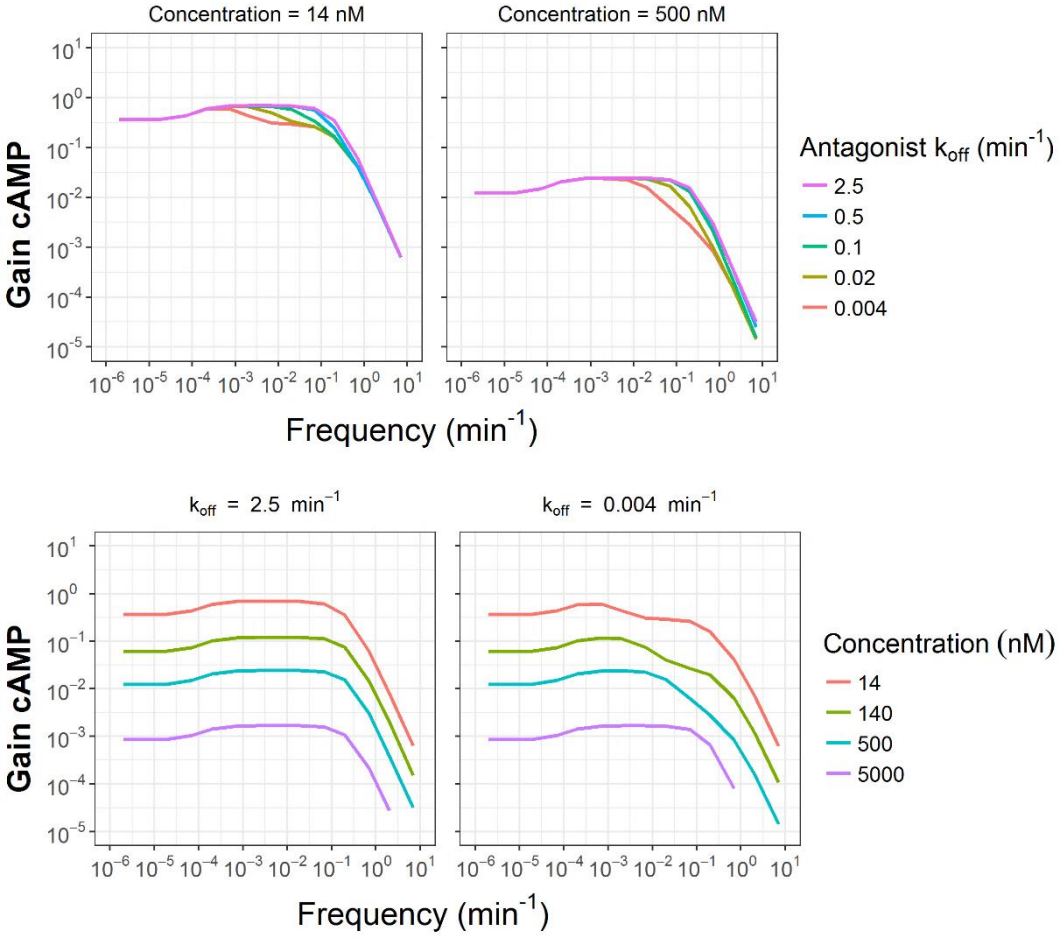

Figure S 8. Frequency response analysis for antagonist concentrations of 14 nM (left) and 500 nM (right). The input signal was a sine wave of free dopamine with an amplitude of 10nM and baseline of 20 nM, at the frequencies indicated on the x-axis. At each antagonist concentration, 5 different antagonist k_{off} values were simulated, which are represented by the different line colors. The k_{on} values were changed simultaneously with k_{off}, which means that the K_D was constant at 6.93 nM. The antagonist concentration was 14 nM, the LFR_{50} was 1.03 and all system-specific parameters were identical to Table 3. The order of the lines in the legend follows the order of the lines in the graph.